UNCLASSIFIED
SECURITY CLASSIFICATION OF THIS PAGE

(2)

DOCUMENTATION PAGE

Form Approved
OMB No. 0704-0188

AD-A199 627

1b. RESTRICTIVE MARKINGS

3. DISTRIBUTION/AVAILABILITY OF REPORT
Approved for public release; distribution is unlimited.

4. PERFORMING ORGANIZATION REPORT NUMBER(S)

5. MONITORING ORGANIZATION REPORT NUMBER(S)
AFOSR-TR- 88-1000

6a. NAME OF PERFORMING ORGANIZATION	6b. OFFICE SYMBOL (If applicable)	7a. NAME OF MONITORING ORGANIZATION
Univ of California		AFOSR/NP

6c. ADDRESS (City, State, and ZIP Code)	7b. ADDRESS (City, State, and ZIP Code)
Los Angeles, CA 90024	Building 410, Bolling AFB DC 20332-6448

8a. NAME OF FUNDING/SPONSORING ORGANIZATION	8b. OFFICE SYMBOL (If applicable)	9. PROCUREMENT INSTRUMENT IDENTIFICATION NUMBER
AFOSR	NP	F49620-85-K-0021

8c. ADDRESS (City, State, and ZIP Code)	10. SOURCE OF FUNDING NUMBERS			
	PROGRAM ELEMENT NO.	PROJECT NO.	TASK NO.	WORK UNIT ACCESSION NO.
Building 410, Bolling AFB DC 20332-6448	61102F	2301	A8	

11. TITLE (Include Security Classification) Computer Simulations of Radiation (U) Generation From Relativistic Electron Beams

12. PERSONAL AUTHOR(S)
Dr. Anthony T. Lin

13a. TYPE OF REPORT	13b. TIME COVERED	14. DATE OF REPORT (Year, Month, Day)	15. PAGE COUNT
FINAL	FROM 10/1/85 TO 9/30/87	10-1-85 to 9-30-87	90

16. SUPPLEMENTARY NOTATION

17. COSATI CODES			18. SUBJECT TERMS (Continue on reverse if necessary and identify by block number)
FIELD	GROUP	SUB-GROUP	
	20.09		Electron Cyclotron Autoresonance Maser, Free Electron Laser
	20.05		

19. ABSTRACT (Continue on reverse if necessary and identify by block number)

Research into mode competition in the Lowbitron and efficiency enhancement through magnetic field profiling; a novel method of gain and efficiency enhancement in the CARM (Electron Cyclotron Autoresonance Maser) which makes use of a transverse helical wiggler to inhibit parasitic autoresonant acceleration of electrons by the electromagnetic wave; absolute instability and tunability of the CARM through varying the solenoidal field; and cyclotron effective in an FEL (Free Electron Laser) with an axial guide magnetic field was carried out. The technical specification for a CARM oscillator in the megawatt power range, with the aim of designing a cost effective experiment utilizing an existing Magnetron Injection Gun and a gyrotron magnet, which will serve to verify the basic physics of the CARM and demonstrate its viability was also investigated. Extensive use of computer simulations using relativistic, electromagnetic PIC codes was made in this study.

20. DISTRIBUTION/AVAILABILITY OF ABSTRACT	21. ABSTRACT SECURITY CLASSIFICATION
☒ UNCLASSIFIED/UNLIMITED ☒ SAME AS RPT. ☐ DTIC USERS	UNCLASSIFIED

22a. NAME OF RESPONSIBLE INDIVIDUAL	22b. TELEPHONE (Include Area Code)	22c. OFFICE SYMBOL
R J BARKER	(202) 767-5011	AFOSR/NP

DD Form 1473, JUN 86 *Previous editions are obsolete.* SECURITY CLASSIFICATION OF THIS PAGE

UNCLASSIFIED

88 10 5 307

COMPUTER SIMULATIONS OF RADIATION GENERATION FROM RELATIVISTIC ELECTRON BEAMS

F49620-85-K-0021

FINAL TECHNICAL REPORT

TO

AIR FORCE OFFICE OF SCIENTIFIC RESEARCH

Dr. Anthony T. Lin

Department of Physics
University of California, Los Angeles
Los Angeles, CA 90024

10-1-85 to 9-30-87

TABLE OF CONTENTS

J

A-1

I. Introduction

This is the final report on work performed under the support of AFOSR Grant F49620-85-K-0021 during the period 1 Oct. 1985 to 30 Sept. 1987. The investigation covered the generation of radiation from relativistic electron beams. The scope and findings of the investigation are summarized in section II. Further details of this work, in reviewed papers, preprints and reports, are appended.

II. Summary of Work Accomplished

During the funding period 1 Oct. 1985 to 30 Sept. 1987, we carried out AFOSR supported research into mode competiton in the Lowbitron and efficiency enhancement through magnetic field profiling; a novel method of gain and efficiency enhancement in the CARM (Electron Cyclotron Autoresonance Maser) which makes use of a transverse helical wiggler to inhibit parasitic autoresonant acceleration of electrons by the electromagnetic wave; absolute instablility and tunability of the CARM through varying the solenoidal field; and cyclotron effects in an FEL (Free Electron Laser) with an axial guide magnetic field. We also investigated the technical specifications for a CARM oscillator in the megawatt power range, with the aim of designing a cost effective experiment utilising an existing Magnetron Injection Gun and a gyrotron magnet, which will serve to verify the basic physics of the CARM and demonstrate its viability. Extensive use of computer simulations using relativistic, electromagnetic PIC codes was made in these studies.

II.1 Mode Competition in the Lowbitron

The lowbitron is a Doppler-shift dominated cyclotron maser with a longitudinal wiggler field such that the net magnetic field is of the form, $\vec{B} = \hat{z}(B_c + B_w Sink_w z)$, where B_w and B_c are respectively, the wiggler and solenoidal fields.[1,2] The lowbitron has certain attractive features. It is capable of generating coherent radiation at a frequency $\omega = (k+k_w)v_z + \Omega_c \approx 2\gamma^2(k_w v_z + \Omega_c)$, where v_z is the beam velocity along the solenoidal field and Ω_c is the relativistic cyclotron frequency. This output frequency is higher than that produced by a free electron laser with the same wiggler modulation, k_w, or that produced by a Doppler-shift dominated cyclotron maser with the same Ω_c. Furthermore, it has the practical advantage in that the longitudinal wiggler is easier to produce, and the wiggler modulation easier to change, than is the case with the transverse wiggler in an FEL. However, it had been thought that the efficiency of this device would be low.

A $1^2/_2$-d particle code[3] has been used to study the lowbitron. The simulations (Appendix 1) show that the cyclotron mode $\omega = kv_z + \Omega_c$, and the lowbitron mode $\omega = (k+k_w)v_z + \Omega_c$ can be simultaneously excited by the electron beam. Competition between these two modes lead to a finite threshold in B_w/B_c for efficient operation. Figure 1 shows the efficiency and growth rate as a function of B_w. The growth rate initially decreases as B_w increases, until a threshold at $B_w \tilde{} B_c/2$ is exceeded, after which the growth rate increases linearly with B_w and the lowbitron mode dominates. Efficiency as high as 25% is attained in the simulations.

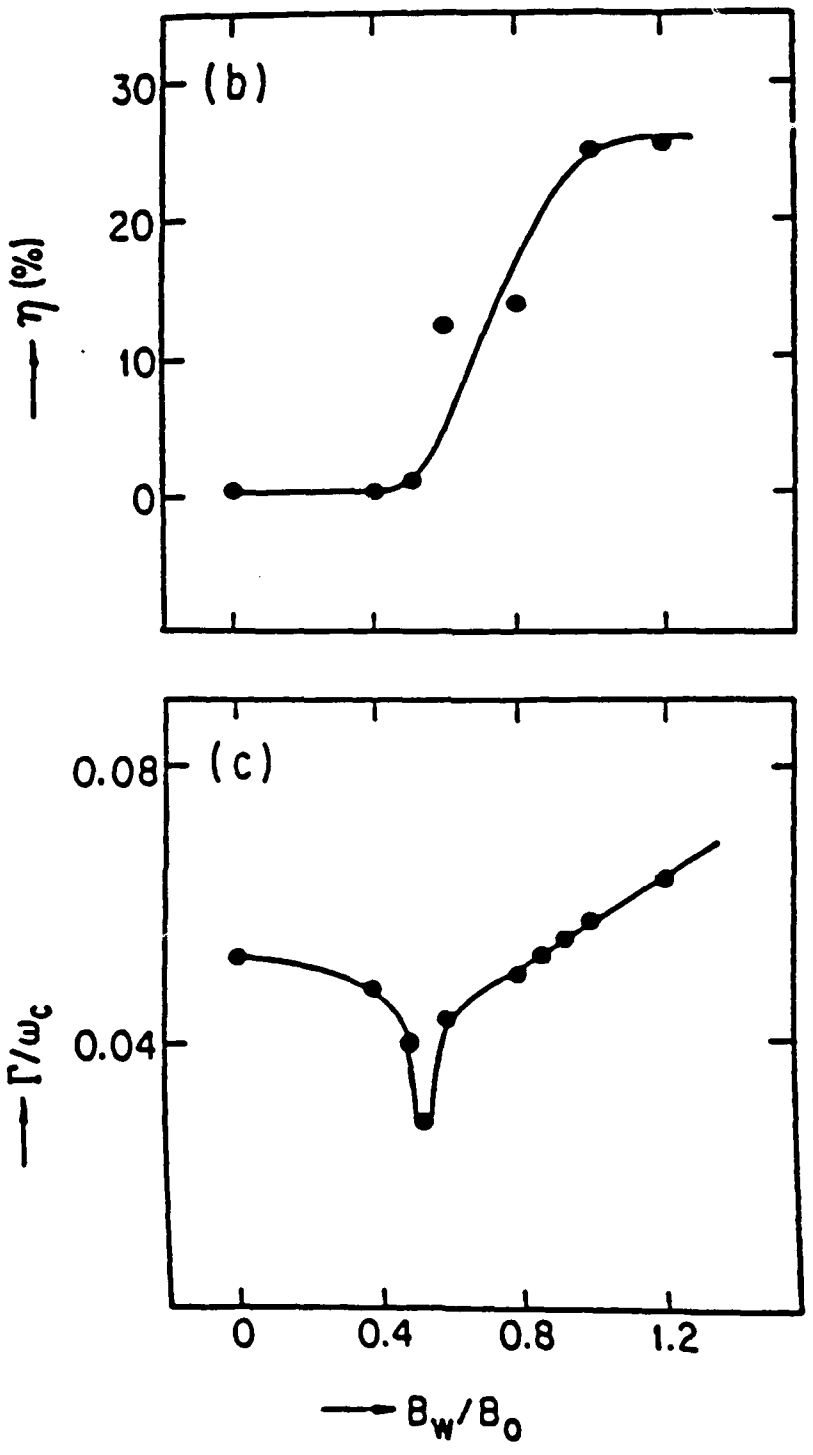

Figure 1

II.2 A High-Efficiency Lowbitron

The efficiency of the lowbitron can be further increased with appropriate tapering of the solenoidal field to prolong the deceleration phase of the electron-wave interaction. The dynamic phase shift of the lowbitron is given by $\Delta\Phi = [\ (k+k_w)\Delta v_z - (\Omega_c/\gamma)\Delta\gamma\ ]t$, where t is the electron transit time in the interaction region. As the rate of change of phase due to v_z and γ are not, in general, equal, the electron eventually drifts into the acceleration phase with respect to the wave, and so ceases the transfer of energy to the wave. To prolong the deceleration phase, the solenoidal field can be tapered so that $\Delta\Phi$ remains small. We find that it is possible to raise the untapered field efficiency of 25% to more than 40% by increasing the solenoidal field with time.

II.3 Enhancemant of Gain and Efficiency in a CARM

The Doppler-shift dominated cyclotron autoresonance maser (CARM) is an attractive source of coherent radiation in the millimeter and submillimeter wavelength range.[4] It possesses a favourable ouput frequency scaling with electron beam energy, as well as the potential for high efficiency. The wave frequency for resonant wave-electron interaction is $\omega=kv_z+\Omega_c$, which scales approximately with the beam kinetic energy as $\omega\approx\gamma^2\Omega_c$, γ, being the Lorentz factor of the beam. For relativistic phase velocity $v_p=\omega/k\approx c$, the change in Ω_c is largely compensated by the change in the Doppler term when an electron interacts with the wave. This phase-locking mechanism between electron and wave provides the basis for high efficiency. However, one drawback is that the gain decreases as $v_p\rightarrow c$. Recalling that an electron can lose as well as

gain energy in its interaction with the wave, the decrease in gain can be viewed as increasing competition between the processes of stimulated electron emission and absorption.

We have found that both the gain and efficiency can be significantly enhanced by adding a transverse helical wiggler field to the CARM in the interaction region. The wiggler field is that produced by a bifilar current winding used in present free electron lasers, given by the model equation $\vec{B}_w=B_w(\hat{x}Cosk_wz + \hat{y}Sink_wz)$. (The net static magnetic field configuration is the same as that in an FEL with a guide magnetic field, but unlike the FEL, the electron beam is injected into the wiggler region with a finite transverse velocity.) The wiggler is used to effect selective inhibition of autoresonance acceleration of electrons (or stimulated absorption) by the wave. In the combined wiggler and uniform axial magnetic field, the unperturbed electron velocity has an oscillating component, $v_z=v_o+\mu Cos(\Omega_c-k_wv_o)$, where v_o is the mean value and $\mu\propto(\Omega_c-k_wv_o)^{-1}$ is small, away from gyroresonance ($\Omega_c=k_wv_o$). By choosing appropriate values for B_w and k_w, it may be arranged such that electrons that undergo autoresonance acceleration will approach gyrosonance, acquiring large oscillations in v_z which quickly detune the electrons from resonance with the wave, and thereby, terminating the acceleration process. On the other hand, electrons that lose energy to the wave will suffer less perturbation in v_z, allowing them to stay locked in phase with the wave. Further details of this enhancement mechanism are given in Appendix 3. One and $^2/_2$-d particle simulations show that significant enhancement in gain and efficiency might be achieved. Figure 2 shows an example of the efficiency and gain in a CARM with (solid dots), and without (hollow dots) a wiggler field, as a function of the wave phase velocity $\beta_p=\omega/kc$.

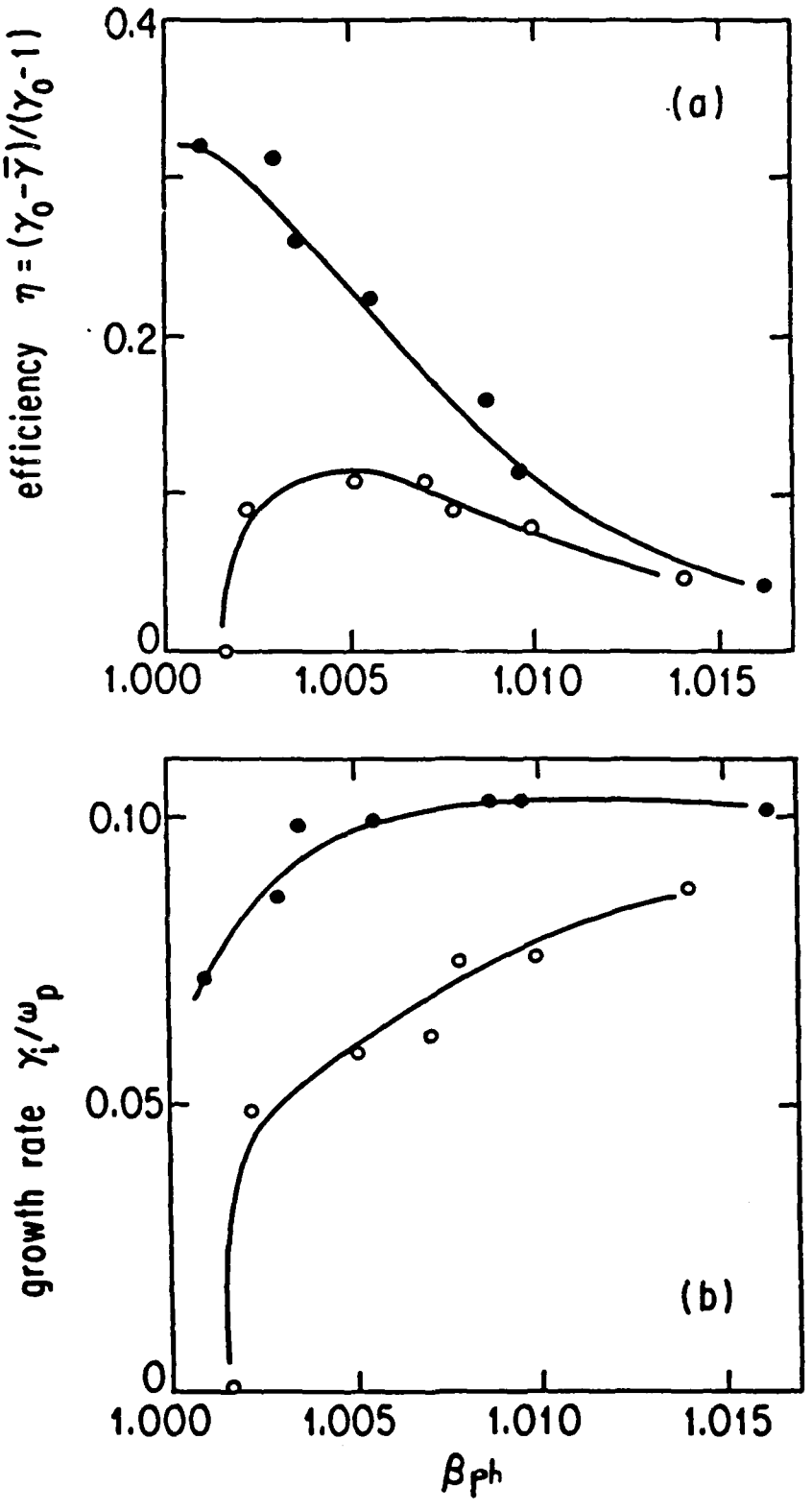
0.4
0.2
0
efficiency $\eta = (\gamma_0 - \bar{\gamma})/(\gamma_0 - 1)$
(a)
1.000
1.005
1.010
1.015
0.10
0.05
0
growth rate γ_i/ω_p
(b)
1.000
1.005
1.010
1.015
β_{ph}

Figure 2

II.4 Stability and Tunability of a CARM Amplifier

Frequency tunability of a CARM amplifier may be achieved by varying either the electron beam energy or the magnetic field. The viability of the latter scheme has been investigated using theoretical analysis and computer simulations. Stability consideration dictates an upper limit to the magnetic field that can be used to upshift the frequency in a CARM. If the cyclotron frequency is too high, the cyclotron mode can excite a low frequency back propagating wave, as well as the desired high frequency forward propagating wave, resulting in an absolute instability (oscillation). One way of suppressing the oscillation is to use a resistively coated waveguide. An example, using a TE_{01} mode, and an electron beam with the parameters (767keV, 2.5kA, $v_\perp/c=0.4$) is considered. Analytic theory developed by Briggs[5] and Chu et al[6] is used to predict the threshold for the absolute instability. It is found that a 40-60% variation of the magnetic field can be achieved for a maximum wall resistivity, parameterized by $\delta=0.01$, where δ is the ratio of wall skin depth to wall radius. A 40% variation in the magnetic field, however, can lead to a frequency tuning range of over 100%. Computer simulations for these beam parameters show linear growth rates in good agreement with theory. Efficiency in excess of 20% can be achived before wave saturation by electron phase trapping. The effects of beam momentum spread are also studied in the computer simulations. They indicate that high beam quality is crucial at high operating frequency. The CARM ceases to be an attractive device for beam momentum spread greater than 3%. Further details are given in Appendix 4.

II.5 CARM Oscillator Design and Analysis

Investigations into the CARM to date have been confined mostly to theoretical studies. In light of the favorable theoretical expectations, it is of pressing interest to design a specific experiment which would allow verification of our understanding of the basic physics of the CARM and demonstrate its viability as a practical device. With these aims in mind, we have initiated a study into the technical specifications for a cost effective CARM oscillator. The CARM oscillator would operate in the megawatt power range and would make use of an existing Magnetron Gun and gyrotron magnet. The study analysed design of the Bragg reflector and resonant cavity. Mode competition with the backward wave is expected to be a important problem and this was analysed for specific oscillator configurations. Based on the analysis, a tentative design for a CARM oscillator is as follows:

voltage	400	kV
current	25	A
$v_\perp/v_z$	0.92	
operating frequency	150	GHz
cavity Q	376	
cavity length	5.1	cm
cavity radius	29	cm
axial magnetic field	37	kG
beam fill factor	40%	

II.6 Hybrid Cyclotron instability in an FEL with Axial Guide Field

From simulations using a $1^2/_2$-d particle code, it is found that a hybrid cyclotron instability can be excited at $\omega=(k+2k_w)v_o-\Omega_c$, with relatively large growth rate and high efficiency. This instability may be explained by the following simple picture. In the combined wiggler and axial magnetic field, the beam electrons have a natural frequency of axial oscillations, given approximately by $\omega'=|\Omega_c-k_w v_o|$ (asuming a right helical wiggler). An electromagnetic wave with frequency $\omega=(k+2k_w)v_o-\Omega_c$ will produce an axial ponderomotive force at the resonant frequency of electron axial oscillations. The resonant ponderomotive force can lead to large amplitude oscillations in the electron axial velocities, which, in turn, is coupled through the wiggler field to give rise to a transverse current which reinforces the wave at $\omega=(k+2k_w)v_o-\Omega_c$. The existence of a natural frequency of oscillation in the electron motion was first pointed out in an earlier analytic work by Friedland and Hirshfield.[7] They were primarily concerned with using this effect to enhance the free electron laser gain very close to gyroresonance, or the unstable beam propagation condition (at gyresonance, the frequencies of th hybrid and FEL mode ($\omega=(k+k_w)v_o$) become the same). Subsequent authors[8,9] have also ignored the existence of a separate hybrid mode. Results from our simulations (see Appendix 6) show that the hybrid mode can be distinguish from the FEL mode. Also, and more importantly, an autoresonance effect appear to occur under certain circumstances, giving rise to high efficiency (>30%) for the hybrid mode. This hybrid mode may lead to new versatility for the free electron laser.

II.B. AFOSR Supported Publications

1. Lin, A.T. and Lin, Chih-Chien, "Competition of Electron Cyclotron Maser and Free Electron Laser Modes with Combined Soelnoidal and Longitudinal Wiggler Fields," Phys. Fluids 29 1348 (1986).

2. Lin, A.T. and Lin, Chih-Chien, "A Highly Efficient Electron Cyclotron Maser Immersed in a Longitudinal Wiggler," Proceedings of The 6th International Conference on High-Power Particle Beams, Kobe, Japan, 1986, page 539.

3. Kho, T.H. and Lin, A.T., "Hybrid FEL-Cyclotron Instability in a Free Elelctron Laser with an Axial Magnetic Field," Int. J. Infrared and MM Waves 8(7) 753 (1987).

4. Kho, T.H. and Lin, A.T., "Enhancement of Gain and Efficiency in an Electron Cyclotron Autoresonance Maser," Phys. Rev. Lett. 59(11) 1181 (1987).

5. Lin, A.T., Chu, K.R., and Bromborsky, "Stability and Tunability of a CARM Amplifier," submitted to IEEE Plasma Science, special issue on High Power Microwave (1987).

References

1. W.A. McMullin and G. Bekefi, Phys. Rev. A 25 1826 (1982).

2. R.C. Davidson and W.A. McMullin, Phys. Fluids 26 840 (1983).

3. A.T. Lin, J.M. Dawson and H. Okuda, Phys. Fluids 17 1995 (1974).

4. A.T. Lin, Int. J. Electron. 57 1097 (1984).

5. R.J. Briggs, "Electron Stream Interaction with Plasma," MIT Press, Cambridge, M.A. (1964), chapter 2.

6. K.R. Chu, A.T. Drobot, H.H. Szu and P. Sprangle, IEEE Trans. Microwave Theory and Techniques, MTT-28, 313 (1980).

7. L. Friedland and J.L. Hirshfield, Phys. Rev. Lett. 22 1456 (1980).

8. W.A. McMullin and R.C Davidson, Phys. Rev. A 25 3130 (1982).

9. H.P. Freund, et al, Phys. Rev. A 26 2004 (1982).

APPENDIX

1. Competition of electron-cyclotron maser and free-electron laser modes with combined solenoidal and longitudinal wiggler fields.
2. A highly efficient electron cyclotron maser immersed in a longitudinal wiggler.
3. Enhancement of Efficiency and Gain in Cyclotron Autoresonance Masers.
4. Stability and Tunability of a CARM Amplifier.

5a. Preliminary Design for a 30 MW CARM Oscillator.

5b. CARM Oscillator Study.

6. Hybrid Cyclotron instability in a Free Electron Laser with an axial magnetic field.

APPENDIX 1

Competition of electron-cyclotron maser and free-electron laser modes with combined solenoidal and longitudinal wiggler fields

A. T. Lin and Chih-Chien Lin
Department of Physics, University of California at Los Angeles, Los Angeles, California 90024

(Received 26 December 1985; accepted 7 February 1986)

A relativistic electron beam with a finite transverse dc momentum ($\beta_\perp = 1/\gamma_0$) passing through a region of combined uniform solenoidal and longitudinal wiggler magnetic fields is observed to convert 25% of its kinetic energy into coherent radiation at frequency $\omega = \gamma_0^2(k_w V_0 + \Omega_c/\gamma_0)$ if the phase velocity of the generated wave is slightly above the speed of light. In this situation, the bunchings of the slow electron-cyclotron mode and free-electron laser modes with combined solenoidal and longitudinal wiggler fields (lowbitron) are observed to compensate each other, which gives rise to a finite threshold for lowbitron operation. In order to attain high efficiency, the wiggler strength of a lowbitron must substantially exceed the threshold.

In the millimeter and submillimeter wavelength ranges, the free-electron devices being actively pursued at many institutions include the gyrotron,[1] Doppler-shift-dominated cyclotron maser,[2-3] and free-electron laser.[4-5] In all these devices, the energy exchange process is one of converting relativistic electron beam kinetic energy into coherent radiation energy by slowing the electrons down through electromagnetic forces. In order for electrons to give up their energy efficiently, they must be bunched in the decelerating phase of the generated wave and remain in this favorable phase as long as possible. The bunching force can come either from a fast wave or a slow wave. In these wavelength ranges, most experimental efforts are concentrated on gyrotrons and free-electron lasers. However, a very attractive alternative to these devices is the Doppler-shift-dominated cyclotron maser. This mechanism for generating microwave radiation possesses the potential of achieving high efficiency, as well as a favorable output frequency scaling with the electron beam energy. Recently it has been shown theoretically[6,7] that a relativistic electron beam with a finite transverse dc momentum passing through a region of combined uniform solenoidal and longitudinal wiggler magnetic fields (lowbitron) is capable of generating coherent radiation at frequency $\omega \approx 2\gamma_0^2(k_w V_0 + \Omega_c/\gamma_0)$, where Ω_c and V_0 are, respectively, the solenoidal field electron-cyclotron frequency and electron axial velocity, k_w is the wiggler wavenumber, and γ_0 is the electron relativistic factor. The output frequency is tunable by varying the electron beam energy and is higher than the frequency from either a free-electron laser with the same wiggler wave number or a Doppler-shift-dominated cyclotron maser with the same solenoidal field. However, the energy conversion mechanism is thought to be a low-efficiency process. On the other hand, it has been demonstrated[3] through computer simulations that a Doppler-shift-dominated cyclotron maser operated in an autoresonant region can convert 25% of the beam kinetic energy into coherent radiation. In this paper, we carry out computer simulations to show that using the magnetic configuration described above also has the potential to achieve high efficiency.

Consider a thin pencil beam of relativistic electrons that traverses on axis through a magnetic field region of the form

$$\mathbf{B} = \hat{z}(B_0 + B_w \sin k_w z). \tag{1}$$

The strength of the solenoidal (B_0) and wiggler (B_w) magnetic fields can be comparable in experiment. The electron transverse motion under the influence of the magnetic field expressed by Eq. (1) is a superposition of Larmor and wiggler motion so that a transverse electromagnetic wave (ω,k) becomes resonant with the electron motion if the following condition is satisfied:

$$\omega = (k_z + k_w)v_z + \Omega_c/\gamma. \tag{2}$$

In emitting a transverse electromagnetic wave propagating along the axial direction, an electron resulting from the recoil of wave momentum will lose both its energy and axial momentum such that

$$\frac{d\Sigma}{dt} = v_{ph}\frac{dP_z}{dt}, \tag{3}$$

where $\Sigma = m_0c^2\gamma$ and v_{ph} is the phase velocity of the wave. Replacing P_z by $m_0\gamma v_z$ in Eq. (3) yields

$$\Delta\gamma = \gamma_0\beta_{ph}\Delta\beta_z/(1-\beta_{ph}\beta_0), \tag{4}$$

where $\beta = v/c$. In order for an electron interacting with a wave to lose its energy as well as its axial velocity, V_0 must be less than c^2/v_{ph}. In this situation, the phase shifts caused by the Doppler and cyclotron terms will compensate each other. In doing so, the electron can remain in resonance with the wave for a long time, and it converts most of its kinetic energy into radiation. The compensation becomes exact if the phase velocity is close to the speed of light and the resonance condition is fulfilled initially. This can be seen by examining the expression for the dynamic phase shift,

$$\Delta\phi = -[(k_z + k_w)\Delta v_z + \Omega_c\Delta(1/\gamma)]T, \tag{5}$$

where T is the electron transit time in the interaction space. Substituting Eqs. (2) and (4) into Eq. (5) yields

$$\Delta\phi = \frac{\Delta\gamma}{\gamma}\left\{\left[\frac{\Omega_c}{\gamma}\left(1-\frac{1}{\beta_{ph}^2}\right) - \frac{k_w c}{\beta_{ph}}(1-\beta_0\beta_{ph})\right] \times\left(1-\frac{\beta_0}{\beta_{ph}}\right)^{-1}\right\}T. \tag{6}$$

Since the second term of Eq. (6) must be negative for an electron to lose both its energy and axial velocity at the same

 0031-9171/86/051348-04$01.90

time, the phase velocity of the generated wave must be greater than the speed of light for the dynamic phase shift to remain small. In a lowbitron, the condition for $\Delta\phi$ to be zero is no longer $V_{ph} = c$ but is $V_{ph} > c$. This is to compensate the phase shift arising from an electron executing wiggler motion in a longitudinal wiggler field.

Without the longitudinal wiggler field, the relativistic electron beam with a finite dc transverse momentum propagating through a region of uniform solenoidal field is already unstable with respect to electron-cyclotron maser instability. The introduction of a longitudinal wiggler field will be considered as a perturbation to the original unstable system. The dispersion relation of the electron-cyclotron mode can be expressed as[8]

$$\omega^2 - k_z^2 c^2 = \frac{\omega_p^2}{\gamma_0}\left(\frac{\omega - k_z v_0}{\omega - k_z v_0 - \Omega_c/\gamma_0} - \frac{\beta_\perp^2(\omega^2 - k_z^2 c^2)}{2(\omega - k_z v_0 - \Omega_c/\gamma_0)^2}\right), \tag{7}$$

where ω_p is the plasma frequency of the electron beam. There are two types of instabilities with different bunching mechanisms. In the regime of $V_{ph} > c$ (fast wave), the bunching mechanism depends on azimuthal electron bunching caused by the relativistic change in electron mass when electrons interact with the transverse electric field of the wave (the so-called negative mass effect). Since an electron gyrates faster in a magnetic field as it loses energy, the electrons initially tend to bunch in phases where the electric force ahead is accelerating and that behind is decelerating. If the Doppler-shifted wave frequency is slightly larger than the relativistic electron-cyclotron frequency, the electron bunches slip behind the wave in phase and on average transfer their energy to the wave. On the other hand, for the case of $V_{ph} < c$ (slow wave), the longitudinal Lorentz force produced by the cross product of the electron dc transverse velocity and the magnetic field of the wave provides the necessary bunching. The electrons initially tend to bunch in regions where the force ahead is decelerating and the force behind is accelerating. If the Doppler-shifted wave frequency is slightly smaller than the relativistic electron-cyclotron frequency, the electron bunches gain on the wave in phase and on average transfer their energy to the electromagnetic wave. Therefore, the electron bunching for the fast-wave and the slow-wave branches should take place 180° out of phase in the electron phase space. According to Eq. (2), the imposition of a longitudinal wiggler field will shift the phase of electron bunching by roughly $k_w V_0$.

In order to investigate the effects of a longitudinal wiggler on the gain and efficiency of an electron-cyclotron maser, a one-and-two-halves-dimensional relativistic electromagnetic particle code[9] is used. The following parameters are chosen: $\gamma_0 = 2.5$, $\beta_\perp = 1/\gamma_0$, $\omega_p = 0.35\omega_c$, $k_w V_0 = 0.81\omega_c$, and $\omega_c = \Omega_c/\gamma_0$. In order to attain high efficiency, the electrons must remain in resonance with the wave for a long time, so a single mode operation is essential. This can be accomplished by using either a Bragg's resonator for an oscillator configuration or injecting a signal with intensity well above the noise level in an amplifier configuration. Only the results of single k mode simulation will be given. The phase velocity of the generated wave and the wiggler strength are varied to determine the parameters for achieving high efficiency. The electron phase-space structure [$(\gamma - 1)$ vs $\phi = \omega_r t - k_z z_l - \tan^{-1}(P_y/P_x)$] at the time when substantial electron bunching has occurred is displayed in Fig. 1. The results of $B_w = 0$ are shown in Fig. 1(a) for a fast wave ($V_{ph} = 1.037c$) and Fig. 1(b) for a slow wave ($V_{ph} = 0.93c$). It is very clear that the phase of electron bunching for these two branches differs by 180°.

By increasing the amplitude of the wiggler field, the lowbitron mode with $\omega_{lb} = (k + k_w)V_0 + \Omega_c/\gamma_0$ will gradually become dominant over the electron-cyclotron maser mode with $\omega_{cm} = kV_0 + \Omega_c/\gamma_0$. In order to investigate the effects of their competition on the gain and efficiency, a series of simulations varying the wiggler field from $B_w = 0$ to $B_w = 1.2B_0$ has been caried out. The wavenumber is chosen to be $kc = 9.8\omega_c$ [Fig. 1(b)] so that $V_{ph} = \omega_{lb}/k = 1.004c$, which meets the condition of autoresonance of Eq. (6). The time evolution of the generated wave energy for two typical cases ($B_w = 0$ and $B_w = B_0$) is shown in Fig. 2(a). For the case of $B_w = 0$, the wave energy exhibits an exponential growth at early time with a growth rate of $\omega_i = 0.051\omega_c$, which is close to estimation from Eq. (7) ($\omega_i = 0.055\omega_c$) and saturates at a level that is less than 1% of the beam kinetic energy. The wave energy of the case of $B_w = B_0$ increases with a growth rate of $\omega_i = 0.056\omega_c$, but saturates at a much higher level, which is about 25% of the beam kinetic energy. The growth rate and efficiency as a function of the wiggler strength are given, respectively, in Figs. 2(b) and 2(c). The simulation results reveal that the growth rate first

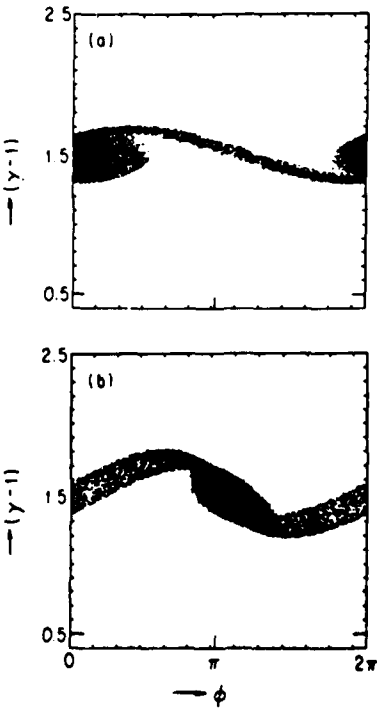

FIG. 1. The phase space of electron-cyclotron maser modes at $\omega_c t = 100$; (a) fast-wave branch ($V_{ph} = 1.037c$) and (b) slow-wave branch ($V_{ph} = 0.93c$).

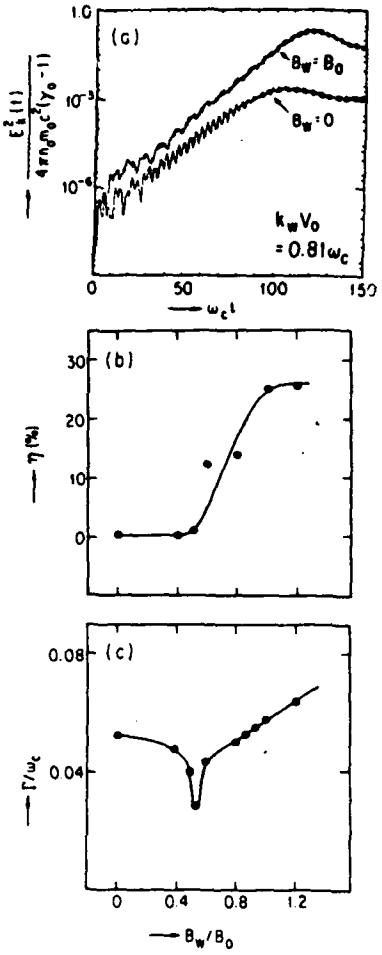

FIG. 2. The effects of longitudinal wiggler on the electron-cyclotron maser instability; (a) the time evolution of the generated wave energy, (b) growth rate versus wiggler strength, and (c) efficiency as a function of wiggler strength.

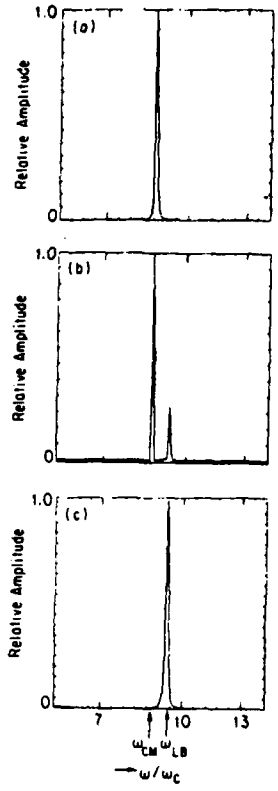

FIG. 3. The frequency spectrum as a function of wiggler strength; (a) $B_w = 0$, (b) $B_w = 0.5B_0$, (c) $B_w = B_0$.

decreases as the wiggler strength is increased until the wiggler strength exceeds a threshold, which in this case is roughly $0.5B_0$. For $B_w > 0.6B_0$, the growth rate increases linearly with the wiggler strength and a lowbitron begins to be able to attain high efficiency.

In order to understand the threshold formation of a lowbitron, consider the wiggler field as a perturbation to the electron-cyclotron maser mode. The increase in wiggler field gradually changes the unstable frequency from the cyclotron maser mode ω_{cm} to the lowbitron mode ω_{lb}. This is demonstrated in Fig. 3, which shows the frequency spectrum as a function of wiggler strength. At $B_w = 0$, the frequency spectrum peaks at the cyclotron maser frequency $\omega = \omega_{cm} = 9.04\omega_c$. With $B_w = 0.5B_0$, two discrete peaks, one at $\omega = \omega_{cm}$ and the other one at $\omega = \omega_{lb} = 9.84\omega_c$, appear in the frequency spectrum. When B_w is increased to B_0, the peak at $\omega = \omega_{lb}$ becomes dominant. According to Eq. (2), there are two discrete frequencies (ω_{cm} and ω_{lb}) for each k mode. Similarly, in an amplifier system, an input ω_0 will excite two modes with discrete wavenumbers. These two modes with a frequency difference of $k_w V_0$ tend to interfere with each other, which gives rise to a finite threshold of the wiggler field for a lowbitron. The time history of electron

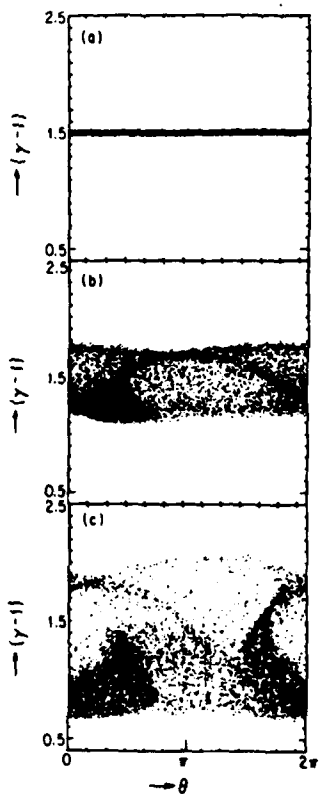

FIG. 4. The time history of phase space for a lowbitron with $B_w = B_0$; (a) $\omega_c t = 0$, (b) $\omega_c t = 100$, (c) $\omega_c t = 120$.

phase space for a lowbitron with $B_w = B_0$ is shown in Fig. 4. The phase of the maximum electron bunching differs from Fig. 1(b) by an amount of roughly $k_w V_0$ [Fig. 4(b)], and Fig. 4(c) indicates that phase trapping is the dominant saturation mechanism.

In conclusion, the competition between the electron-cyclotron maser and lowbitron modes is believed to give rise to a finite threshold for a lowbitron. By choosing the parameters such that $V_{ph} > c$, a lowbitron is capable of attaining high efficiency of the order of 25%.

ACKNOWLEDGMENTS

This work was supported by the Air Force Office of Scientific Research, under Contract No. F 49620-85-K-0021, the Office of Naval Research, and the U. S. Department of Energy, under Contract No. DOE DE-AM03-76SF00010 PA26, Task VIb.

[1] J. L. Hirshfield and V. L. Granatstein, IEEE Trans. Microwave Theory Tech. MTT-25, 522 (1977).
[2] A. T. Lin, Int. J. Electron. 57, 1097 (1984).
[3] V. L. Bratman, N. S. Ginzburg, G. S. Nusinovich, M. I. Petelin, and P. S. Strelkov, Int. J. Electron. 51, 541 (1981).
[4] T. Kwan, J. M. Dawson, and A. T. Lin, Phys. Fluids 20, 581 (1977).
[5] *Free-Electron Generators of Coherent Radiation*, Physics of Quantum Electronics, Vol. 7, edited by S. F. Jacobs, H. S. Pilloff, M. Sargent, M. O. Scully, and R. Spitzer (Addison-Wesley, Cambridge, 1980).
[6] W. A. McMullin and G. Bekefi, Phys. Rev. A 25, 1826 (1982).
[7] R. C. Davidson and W. A. McMullin, Phys. Fluids 26, 840 (1983).
[8] J. L. Hirshfield, K. R. Chu, and S. Kainer, Appl. Phys. Lett. 33, 847 (1948).
[9] J. M. Dawson and A. T. Lin, in *Handbook of Plasma Physics*, edited by A. A. Galeev and R. N. Sudan (North-Holland, Amsterdam, 1984), Vol. II, p. 555.

APPENDIX 2

A HIGHLY EFFICIENT ELECTRON CYCLOTRON MASER IMMERSED IN A LONGITUDINAL WIGGLER

A. T. Lin and Chih-Chien Lin

Department of Physics, University of California
Los Angeles, CA 90024 USA

Abstract

A relativistic electron beam with a finite transverse dc momentum ($\beta_\perp = 1/\gamma_o$) passing through a region of combined uniform solenoidal and longitudinal wiggler magnetic field is observed to convert 25% of its kinetic energy into coherent radiation at frequency $\omega = \gamma_o^2 (k_w V_o + \Omega_c/\gamma_o)$ if the phase velocity of the generated wave is slightly above the speed of light. In order to attain high efficiency, the wiggler strength of a lowbitron must be comparable to the solenoidal field strength. Furthermore, the efficiency can be increased to about 42% if the solenoidal field is properly profiled.

Introduction

In the millimeter and submillimeter wavelength ranges, the free electron devices being actively pursued at many institutions include gyrotron [1], Doppler-shifted dominated cyclotron maser [2] [3], and free electron laser [4] [5]. In all these devices, the energy exchange process is one of converting relativistic electron beam kinetic energy into coherent radiation energy by slowing the electrons down through electromagnetic forces. In order for electrons to give up their energy efficiently, they must be bunched in the decelerating phase of the generated wave and remain in this favorable phase as long as possible. The bunching force can come either from a fast wave or a slow wave. In these wavelength ranges, most experimental efforts are concentrated on gyrotrons and free electron lasers. However, a very attractive alternative to these devices is the Doppler-shift dominated cyclotron maser. This mechanism of generating microwave radiation possesses the potential of achieving high efficiency, as well as a favorable output frequency scaling with the electron beam energy. Recently it has been shown theoretically [6] [7] that a relativistic electron beam with a finite transverse dc momentum passing through a region of combined uniform solenoidal and longitudinal wiggler magnetic fields (lowbitron) is capable of generating coherent radiation at frequency $\omega = 2\gamma_o^2 (k_w V_o + \frac{\Omega_c}{\gamma_o})$ where Ω_c and V_o are respectively the solenoidal field electron cyclotron frequency and electron axial velocity, k_w is the wiggler wave number, and γ_o is the electron relativistic factor. The output frequency is tuneable by varying the electron beam energy and is higher than the frequency from either a free electron laser with the same wiggler wave number or a Doppler-shift dominated cyclotron maser with the same solenoidal field. However, the energy conversion mechanism is thought to be a low efficient process. On the other hand, it has been demonstrated [3] through computer simulations that a Doppler-shift dominated cyclotron maser operated in an auto-resonant region can convert 25% of the beam kinetic energy into coherent radiation. In this paper, we carry out computer simulations to show that using the magnetic configuration described above also has the potential to achieve very high efficiency if the solenoidal magnetic field is properly profiled.

Single Electron Calculation

Consider a thin pencil beam of relativistic electrons traverses on axis through a magnetic field region of the form

$$\vec{B} = \hat{z} (B_o + B_w \sin k_w z) \qquad (1)$$

The strength of the solenoidal (B_o) and wiggler (B_w) magnetic field can be comparable in real experiment. The electron transverse motion under the influence of the magnetic field expressed by Eq. (1) is a superposition of Larmor and wiggler motion so that a transverse electromagnetic wave (ω, k) becomes resonant with the electron motion if the following condition is satisfied:

$$\omega = (k_z + k_w) v_z + \frac{\Omega_c}{\gamma} \qquad (2)$$

In emitting a transverse electromagnetic wave propagating along axial direction an electron due to recoil of wave momentum will lose both its energy and axial momentum such that

$$\frac{d\mathcal{E}}{dt} = v_{ph} \frac{dP_z}{dt} , \tag{3}$$

where $\mathcal{E} = m_o c^2 \gamma$ and v_{ph} is the phase velocity of the wave. Replacing P_z by $m_o \gamma v_z$ in Eq. (3) yields

$$\Delta\gamma = \frac{\gamma_o \beta_{ph} \Delta\beta_z}{1 - \beta_{ph}\beta_o} , \tag{4}$$

where $\vec{\beta} = \frac{\vec{v}}{c}$. In order for an electron interacting with a wave to lose its energy as well as its axial velocity, V_o must be less than $\frac{c^2}{v_{ph}}$. In this situation, the phase shift caused by the Doppler and cyclotron terms will compensate each other. In doing so, the electron can remain in resonance with the wave for a long time and converts most of its kinetic energy into radiation. The compensation becomes exact if the phase velocity is close to the speed of light and the resonance condition is fulfilled initially. This can be seen by examining the expression for the dynamic phase shift

$$\Delta\phi = -\left[(k_z + k_w)\, \Delta v_z + \Omega_c \Delta \left(\frac{1}{\gamma}\right)\right] T , \tag{5}$$

where T is the electron transit time in the interaction space. Substituting Eqs. (2) and (4) into Eq. (5) yeilds

$$\Delta\phi = \frac{\Delta\gamma}{\gamma} \frac{\left[\frac{\Omega_c}{\gamma}\left(1 - \frac{1}{\beta_{ph}^2}\right) - \frac{k_w c}{\beta_{ph}}\left(1 - \beta_o \beta_{ph}\right)\right]}{\left(1 - \frac{\beta_o}{\beta_{ph}}\right)} T. \tag{6}$$

Since the second term of Eq. (6) must be negative for an electron to lose both its energy and axial velocity at the same time, the phase velocity of the generated wave must be greater than the speed of light for the dynamic phase shift to remain small. In a lowbitron, the condition for $\Delta\phi$ to be zero is no longer $V_{ph} = c$ but is $V_{ph} > c$. This is to compensate the phase shift arising from an electron executing wiggler motion in a longitudinal wiggler field.

Electron Cyclotron Maser

Without the longitudinal wiggler field, the relativistic electron beam with a finite dc transverse momentum propagating through a region of uniform solenoidal field is already unstable with respect to electron cyclotron maser instability. The introduction of a longitudinal wiggler field will be considered as a perturbation to the original unstable system. The dispersion relation of electron cyclotron mode can be expressed as [8]

$$\omega^2 - k_z^2 c^2 = \frac{\omega_p^2}{\gamma_o}\left[\frac{\omega - k_z v_o}{\omega - k_z v_o - \frac{\Omega_c}{\gamma_o}} - \frac{\beta_\perp^2 (\omega^2 - k_z^2 c^2)}{2(\omega - k_z v_o - \frac{\Omega_c}{\gamma_o})^2}\right] \tag{7}$$

where ω_p is the plasma frequency of the electron beam. There are two types of instabilities with different bunching mechanism. In the regime of $V_{ph} > c$ (fast wave), the bunching mechanism depends on azimuthal electron bunching caused by the relativistic change in electron mass when electrons interact with the transverse electric field of the wave (the so-called negative mass effect). Since an electron gyrates faster in a magnetic field as it loses energy, the electrons initially tend to bunch in phases where the electric force ahead is accelerating and that behind is decelerating. If the Doppler-shifted wave frequency is slightly larger than the relativistic electron cyclotron frequency, the electron bunches slip behind the wave in phase and on average transfer their energy to the wave. On the other hand, for the case of $V_{ph} < c$ (slow wave), the longitudinal Lorentz force produced by the cross product of the electron dc transverse velocity and the magnetic field of the wave provides the necessary bunching. The electrons initially tends to bunch in regions where the force ahead is decelerating and the force behind is accelerating. If the Doppler-shifted wave frequency is slightly smaller than the relativistic electron cyclotron frequency, the electron bunches gain on the wave in phase and on average transfer their energy to the electromagnetic wave. Therefore, the electron bunching for the fast-wave and the slow-wave branches should take place 180° out of phase in the electron phase space. According to Eq. (2), the imposition of a longitudinal wiggler field will shift the phase of electron bunching by roughly $k_w V_o$.

In order to investigate the effects of a longitudinal wiggler on the gain and efficiency of an electron cyclotron maser, an one and two halves dimensional relativistic electromagnetic particle code [9] is used. The following parameters are chosen: $\gamma_o = 2.5$, $\beta_\perp = \frac{1}{\gamma_o}$, $\omega_p = 0.35\ \omega_c$, $k_w V_o = 0.81\ \omega_c$ and $\omega_c = \frac{\Omega_c}{\gamma_o}$. In order to attain high efficiency, the electrons must remain in resonance with the wave for a long time so a single mode

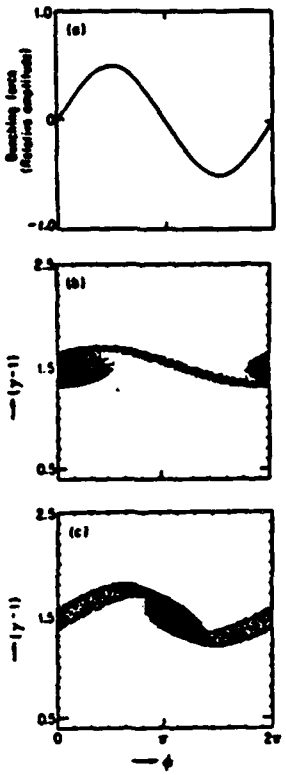

Figure 1. The electron phase of electron cyclotron maser modes relative to the bunching force at $\omega_c t$= 100, (a) bunching force, (b) fast wave branch (V_{ph} =1.037c), (c) slow wave branch (V_{ph}=0.93c).

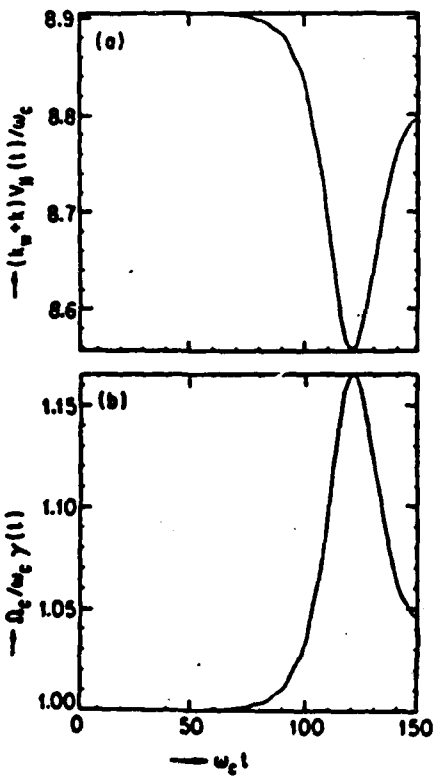

Figure 2. The time evolution of phase shift due to (a) decrease in V_g, (b) decrease in γ of a lowbitron mode.

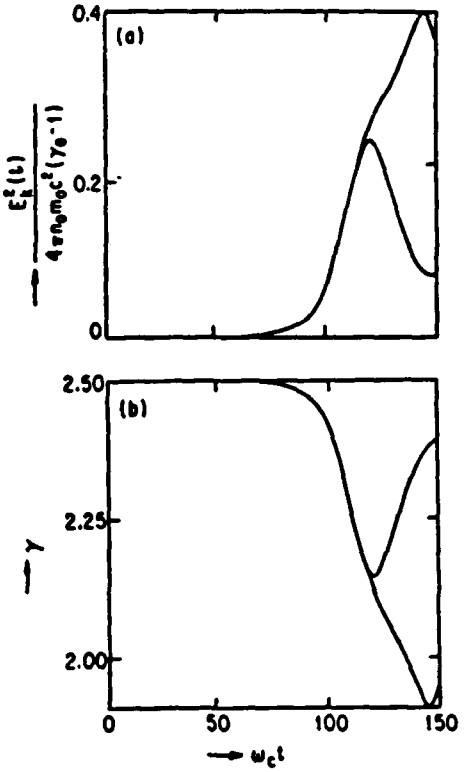

Figure 3. The time evolution of (a) wave energy, (b) electron beam energy, with and without profiling the solenoidal magnetic field.

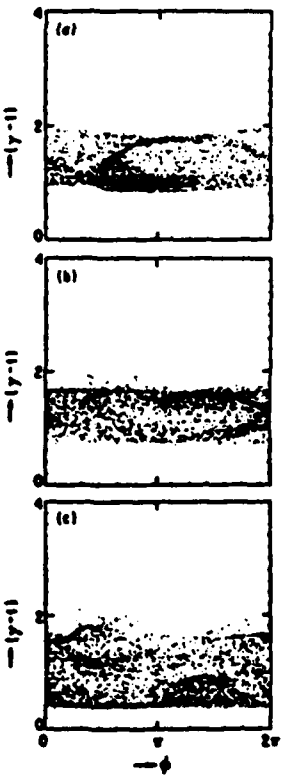

Figure 4. The time history of electron phase space at (a) $\omega_c t$ = 100, (b) $\omega_c t$ = 145 and with constant B_o, (c) $\omega_c t$ = 145 and with varying B_o.

operation is essential. This can be accomplished by using either a Bragg's resonator for an oscillator configuration or injecting a signal with intensity well above the noise level in an amplifier configuration. Only the results of single k mode simulation will be given. The phase velocity of the generated wave and the wiggler strength are varied to determine the parameters for achieving high efficiency. The electron phase space structure $\left((\gamma - 1) \text{ versus } \phi = \omega_r t - k_z z_1 - \tan^{-1}\frac{P_y}{P_x}\right)$ at the time when substantial electron bunching has occured, as well as the bunching force, are displayed in Fig. 1. The results of $B_w = 0$ are shown in Fig. 1b for fast wave ($V_{ph} = 1.037c$) and Fig. 1c for slow wave ($V_{ph} = 0.93c$). It is very clear that the phase of electron bunching for these two branches differs by 180 degrees.

It has been shown in [10] that with $B_w = B_o$ and $V_{ph} = 1.004C$, the lowbitron mode becomes dominated over the electron cyclotron mode and the electron beam is able to convert 25% of its kinetic energy into radiation.

Efficiency Enhancement

As has been explained in the previous section, in order for the electron bunch to start in the decelerating phase, the initial kinetic phase shift between the electrons and electromagnetic wave cannot be zero. At the same time, in order to avoid the exact cancellation of azimuthal and longitudinal inertial bunching, the rate of phase change attributed to the decrease of V_z ($\Delta\phi_1 = (k + k_w)V_z(t)$) and $\gamma(\Delta\phi_2 = \Omega_c/\gamma(t))$ cannot be exactly the same. These two phase shifts eventually will render the electron bunches to be in the accelerating phase and cause the energy conversion process to stop. To prolong the conversion process, $\Delta\phi_1$ can be changed to decrease the dynamic phase shift by properly profiling the solenoidal magnetic field. Figure 2 shows the time evolution of dynamic phase shift. The results reveal that the increase in $\Delta\phi_2$ is faster than the decrease in $\Delta\phi_1$. To slow the change in $\Delta\phi_2$ down, the solenoidal magnetic field $B_o(t)$ for the case of $B_w = B_o(0)$ is linearly increased from $B_o(0)$ to $1.25\ B_o(0)$ during the time span of $\omega_c t = 112$ to $\omega_c t = 126.4$. The time evolution of averaged electron energy (Fig. 3a) and wave energy (Fig. 3b) for both cases with constant B_o and varying $B_o(t)$ are displayed in Fig. 3, which demonstrates that the efficiency can be enhanced from 24% to 42%. For comparision, the time history of electron phase space is shown in Fig. 4. At the time of saturation ($\omega_c t = 145$) for the case of varying solenoidal field, the electrons are mostly in their decelerating phase (Fig. 4c), whereas the electrons are mostly in their accelerating phase (Fig. 4b) without varying B_o.

Summary

In conclusion, by choosing the parameters such that $V_{ph} \geq c$ and $B_w = B_o$ a lowbitron is capable of attaining high efficiency of the order of 25%. Furthermore, the efficiency can be increased to 42% by properly profiling the solenoidal magnetic field.

Acknowledgments

This work was supported by AFOSR F49620-85-K-0021, ONR, and NSF.

References

1. J.L. Hirshfield and V.L. Granatstein, IEEE, TMTT, 25, 522 (1977).
2. A.T. Lin, Int. J. Electronics, 57, 1097 (1984).
3. V.L. Bratman, N.S.Ginzburg, G.S. Nusinovich, M.I. Petelin, and P.S. Strelkov, Int. J. Electronics, 51, 541 (1981).
4. T. Kwan, J.M. Dawson, and A.T. Lin, Phys. Fluids, 20, 581 (1977).
5. Free-Electron Generators of Coherent Radiation, Edited by S.F. Jacobs, H.S. Pilloff, M. Sargent, M.O. Scully, and R. Spitzer, Physics of Quantum Electronics, 7, (1980, Addison-Wesley Publishing Co.)
6. W.A. McMullin and G. Bekefi, Phys. Rev. A., 25, 1826 (1982).
7. R.C. Davidson and W.A. McMullin, Phys. Fluids, 26, 840 (1983).
8. J.L. Hirshfield, K.R. Chu, and S. Kainer, Appl. Phys. Lett. 33, 847 (1948).
9. J.M. Dawson and A.T. Lin, Handbook of Plasma Physics, Vol. II, edited by A.A. Galeev and R.N. Sudan, 555 (1984).
10. A.T. Lin and Chih-Chien Lin, Phys. Fluids, 29, May (1986).

APPENDIX 3

Enhancement of Efficiency and Gain in Cyclotron Autoresonance Masers

T. H. Kho and A. T. Lin
Physics Department, University of California at Los Angeles, Los Angeles, California 90024
(Received 20 April 1987)

A new scheme of enhancing the efficiency and gain of a Doppler-shifted electron-cyclotron autoresonance maser, with use of a transverse magnetic wiggler to inhibit stimulated absorption, is proposed. Computer simulations with use of a $1\frac{1}{2}$-dimensional, electromagnetic, relativistic particle code show significant improvement in the efficiency, and gain may be attained with this scheme.

PACS numbers: 42.52.+x

Advances in high-power, relativistic electron beam technology over the past decade have made the electron-cyclotron maser[1,2] an increasingly attractive source of tunable, coherent radiation in the millimeter and submillimeter wavelength ranges. The radiation is generated by relativistic electrons, which, as a result of the dependence of electron-cyclotron frequency on the relativistic mass, tend to bunch together as they gyrate around a solenoidal magnetic field, $\mathbf{B}_0$.[3] The resonant condition for electron-wave interaction is given approximately by

$$\omega_r = kv_{\parallel} + \Omega_0/\gamma, \tag{1}$$

where $v_{\parallel}$ is the drift velocity of the beam along $\mathbf{B}_0$, $\gamma = (1 - v^2/c^2)^{1/2}$, Ω_0/γ is the relativistic electron-cyclotron frequency, and $v_p = \omega_r/k$ is the phase velocity of the resonant wave. An output frequency much higher than the electron-cyclotron frequency may be obtained by use of highly relativistic beam drift velocity.[4]

A property of electron interaction with the wave is that its velocity, $v_{\parallel}$, is a function of its energy and initial conditions only, regardless of the electromagnetic (EM) wave amplitude[2]:

$$\beta_{\parallel} = [1 - (1 - \beta_{ph}\beta_{\parallel 0})\gamma_0/\gamma]/\beta_{ph}, \tag{2}$$

where $\beta_{\parallel} = v_{\parallel}/c$, $\beta_{ph} = \omega/kc$, $\gamma_0 = \gamma(t_0)$, and $\beta_{\parallel 0} = \beta(t_0)$. This follows from the equations for the electron energy and momentum, $d\xi/dt = -e\mathbf{v}\cdot\mathbf{E}$ and $dp_{\parallel}/dt = -e(\mathbf{v}\cdot\mathbf{E})/v_{ph}$. Equation (2) shows that an electron can lose all its kinetic energy, both transverse and longitudinal, to the wave if its initial drift velocity satisfies $\beta_{\parallel 0} = (\gamma_0 - 1)/\gamma_0\beta_{ph}$. In general, electrons confined to ellipsoidal trajectories in $\beta_{\perp} - \beta_{\parallel}$ phase space $[\beta_{\perp} = (1 - \gamma^{-2} - \beta^2)^{1/2}]$,

$$\beta_{\perp}^2 + \beta_{\parallel}^2 = 1 - [(1 - \beta_{ph}\beta_{\parallel})/\gamma_0(1 - \beta_{ph}\beta_{\parallel 0})]^2, \tag{3}$$

suffer maximum energy loss when they have given up all their transverse momentum. For efficient energy conversion, an electron has to be able to maintain the resonance condition for a sufficiently long time. The phase shift of an electron relative to the wave may be expressed as $\theta(t) = (\delta_k + \delta_d)$, where $\delta_k = (\omega - \omega_r)t$ is the kinetic shift and $\delta_d = -[k\Delta v_{\parallel} + \Omega_0\Delta(1/\gamma)]t$ is the dynamic shift due to electron-wave interaction. With use of Eqs. (1) and (2), δ_d may be expressed as

$$\delta_d = [\omega_r(\Delta\gamma/\gamma_0)][1 - (\omega/\omega_r\beta_{ph}^2)]t. \tag{4}$$

The dynamical shift vanishes if $\beta_{ph}^2 = \omega/\omega_r$, the change in electron-cyclotron frequency being exactly cancelled by the change in Dopper shift due to electron recoil. Therefore, if $\omega = \omega_r$ is initially satisfied, an electron will remain in phase with the EM wave for all times if $\beta_{ph} = 1$. This autoresonant regime holds out the prospect of high efficiency.[5,6]

However, depending on the initial phase of electrons relative to the wave, the autoresonant condition can also lead to acceleration of electrons. Equations (2) and (4) show that an electron can be accelerated indefinitely. The pitch factor of the beam is given by $\beta_{\perp}/\beta_{\parallel} = [2/(\gamma - 1)]^{1/2}$ (for $\beta_{ph} = 1$), so that at large γ, the beam momentum is predominantly along $\mathbf{B}_0$. This acceleration mechanism has attracted attention to its potential application as a high-energy particle accelerator.[7]

The electron-energy loss and gain are the classical correspondents of stimulated emission and absorption. To encourage positive gain in the cyclotron autoresonance maser (CARM), a small initial mismatch in frequency, $\omega > \omega_r$, with $\beta_{ph}^2 > \omega/\omega_r$ is desirable in order to favor stimulated emission over absorption.[2] An examination of the equations for phase shifts above shows that electrons that give up energy to the wave will suffer smaller phase shifts than those that are accelerated by it, with these conditions. Nevertheless, as the wave grows in a conventional CARM, a sizable fraction of the electrons will be accelerated by it and, since wave energy is expended in accelerating these electrons, they depress both the efficiency and gain of the CARM.

In this paper we propose a method of curtailing the autoresonant acceleration of electrons. We show that by imposing a transverse, helical "wiggler" magnetic field onto a conventional CARM, electrons accelerated by the wave can be made to go off resonance with the wave, and, hence, terminate the accleration process, while electrons that lose energy to the wave will remain in resonance with it. Computer simulations demonstrate that

both efficiency and growth rate can be significantly enhanced as a result.

The detuning mechanism arises from the behavior of electrons moving in the combined wiggler and uniform axial magnetic field modeled by

$$\mathbf{B} = B_0\hat{z} + B_w[\hat{x}\cos(k_w z) + \hat{y}\sin(k_w z)],$$

where B_w is the wiggler field strength and k_w its pitch. This wiggler field is an idealization of that produced by a bifilar current winding and currently in use in free-electron laser experiments.[8] Equilibrium electron motion in this magnetostatic field is approximately described by

$$\begin{aligned} v_x &= v_w\cos(k_w z) + v_\perp\cos(\Omega_c t + \phi), \\ v_y &= v_w\sin(k_w z) + v_\perp\sin(\Omega_c t + \phi), \\ v_z &= v_\parallel - \mu\cos(k_w z - \Omega_c t + \phi), \end{aligned} \tag{5}$$

where $v_w = v_\parallel(B_w/B_0)/(1 - k_w v_\parallel/\Omega_c)$, $\mu = v_w v_\perp/v_\parallel$, $\Omega_c = \Omega_0/\gamma$, ϕ is an initial phase, and $\mu/v_\parallel \ll 1$ has been assumed. The electron beam is injected with a finite transverse velocity, $v_\perp$, into the wiggler region. The effect of $\mathbf{B}_w$ is to induce an additional mode of gyration about $\hat{z}$ with a frequency $\Omega \simeq k_w v_\parallel$ and an oscillation in the axial velocity v_z about its mean value $v_\parallel$ at the beat frequency $\Omega \simeq k_w v_\parallel - \Omega_c$.

From Eqs. (2), (3), and (5), we can deduce approximately the variation of μ with $v_\parallel$. This is shown qualitatively in Fig. 1. A singularity occurs at gyroresonance, $k_w v_\parallel = \Omega_c$, in the neighborhood of which Eqs. (5) no longer give an accurate description of electron motion. On either side of the singularity, μ varies monotonically with $v_\parallel$; branch X corresponds to the case $\Omega_c > k_w v_\parallel$ and branch Y to $\Omega_c < k_w v_\parallel$. Figure 1 is also qualitatively representative of the variation of μ with γ, with the transformations $\gamma \to 1$ as $\beta_\parallel \to 0$ and $\gamma \to \infty$ as $\beta_\parallel \to 1$. Assumed in this qualitative description of μ is that the wiggler is sufficiently weak so that the mean $\beta_\parallel$ is still essentially given by Eq. (2). This condition is necessary if we are to use the cyclotron autoresonance effect. Also assumed is that the electron motion can be approximately described by Eq. (5) even in the presence of the EM field (see a discussion of Fig. 3 below).

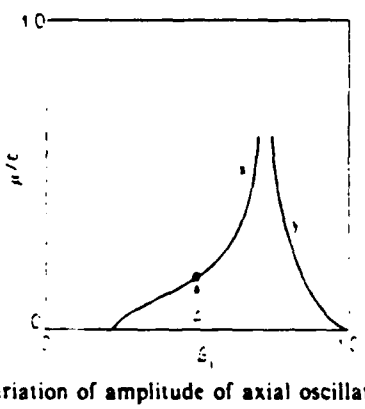

FIG. 1. Variation of amplitude of axial oscillation μ/c with mean velocity, $\beta_\parallel$.

The variation of μ with $v_\parallel$ (and γ) depicted in Fig. 1 can be exploited to provide a discriminate detuning mechanism in the CARM. Consider a CARM with a helical magnetic field such that initially $\Omega_c > k_w v_\parallel$ and the electron beam is described by, for example, point A on curve X. Then electrons accelerated by the wave will move to the right of A, gaining a larger oscillating component in its axial velocity. If the slope at A is sufficiently steep, the increasing axial oscillations will quickly desynchronize these electrons with the wave. On the other hand, electrons losing energy to the wave will move to the left of A, reducing their axial oscillations and, hence, becoming more in resonance with the wave. In short, accelerated electrons become more "noisy" and quickly move out of resonance with the wave, while the opposite process occurs for those electrons that are driving the wave.

To illustrate the mechanism behind this enhancement scheme and its potential, we present below results from computer simulations of a CARM with helical magnetic field using a $1\frac{2}{2}$-dimensional, EM, relativistic particle code with periodic boundary conditions.[9] The electrons are initially monoenergetic with uniform axial velocity, $v_\parallel$ and $v_\perp$, and are uniformly distributed over the transverse phase angle, $\theta = \tan^{-1}(v_x/v_y)$, $-\pi \le \theta < \pi$. The helical field, B_w, is switched on adiabatically to let electrons find their equilibrium orbits. The EM wave is then allowed to grow from noise, with B_w kept constant. Only one k mode of the EM wave is kept in a given simulation. Results are presented below for the following parameters and initial conditions:

$$\gamma_0 = 3, \quad B_w/B_0 = 0.091, \quad \Omega_0/\gamma_0 k_w v_{\parallel 0} = 2.69,$$

$$\Omega_0/\gamma_0\omega_p = 2.33, \quad \beta_{\perp 0} = \gamma_0^{-1},$$

where $\omega_p = (4\pi n_e e^2/m)^{1/2}$. The values correspond to a CARM operating along curve X in Fig. 1. Comparisons are made with simulations with identical initial conditions but with $\mathbf{B}_w = 0$. As $B_w/B_0 \ll 1$, and the initial conditions are removed from gyroresonance, $\mathbf{B}_w$ initially presents only a small perturbation to conventional CARM electron motion.

Figure 2 compares efficiency and growth rate with and without $\mathbf{B}_w$ as a function of β_{ph}, the phase velocity of the excited EM wave. The efficiency is defined as $\eta = (\gamma_0 - \bar{\gamma})/(\gamma_0 - 1)$, where $\bar{\gamma}$ is the value of γ averaged over all electrons at saturation. Substantial improvement in gain and growth rate is evident over a range of β_{ph} slightly greater than 1. The peak efficiency is increased by about a factor of 3 with the inclusion of B_w, from 11% to 32%. The effectiveness of $\mathbf{B}_w$ in suppressing autoresonant acceleration can be seen from Fig. 3, which shows phase plots of kinetic energy $\xi_k = (\gamma - 1)$ vs β for

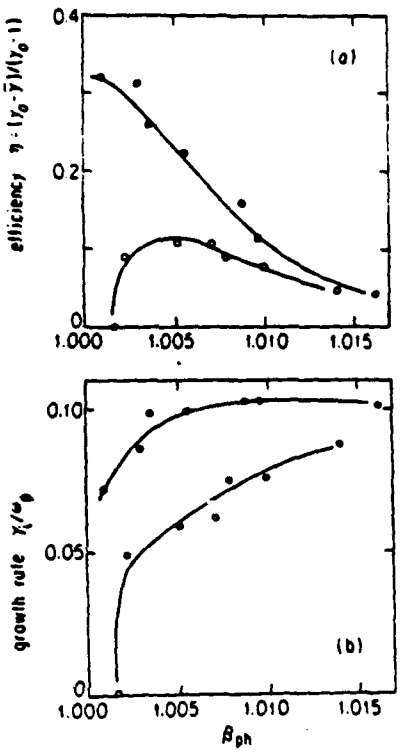

FIG. 2. Comparison of (a) efficiency and (b) growth rate, with (filled circles) and without (open circles) B_w, as a function of the phase velocity $\beta_{ph}=\omega/kc$.

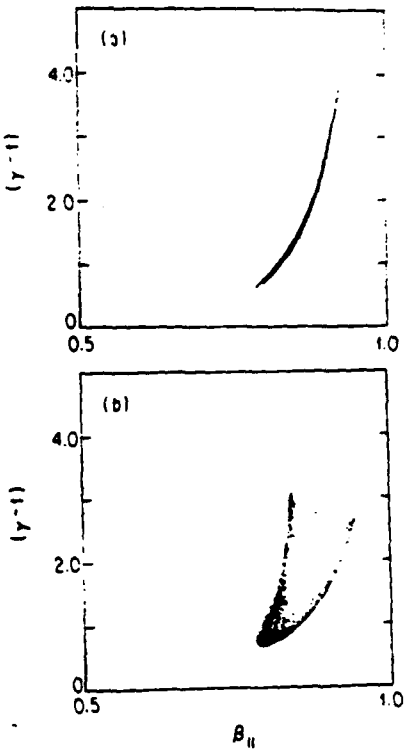

FIG. 3. Phase plots of $(\gamma-1)$ vs $\beta_{\parallel}$ at saturation for $\beta_{ph}\approx 1.002$ (a) with B_w and (b) without B_w.

the case $\beta_{ph}\approx 1.002$ with and without $\mathbf{B}_w$ [the second set of data points from the left-hand side in Fig. 2(a)] at saturation. Without $\mathbf{B}_w$, electrons are distributed along the hyperbola defined by Eq. (2). Initially, all electrons lie at point ($\xi_k=2$, $\beta=\beta_{\parallel 0}$) on this curve. As the EM wave grows, electrons driving the wave move down the curve, while those accelerated by the wave move up the curve. The lower boundary of this curve is defined by the value of $\beta_{\parallel}$ at which an electron loses all transverse momentum. For this example, this occurs at $\beta_{\parallel}\simeq 0.78$, $\xi_k\simeq 0.6$, from Eq. (3). At the upper end of this curve, electrons are accelerated up to $\xi_k\approx 4.5$. Acceleration eventually stops when phase slippage between electron and wave exceeds $\pm\pi$. For the case with $\mathbf{B}_w$, electrons are initially described by a line joining the points ($\xi_k=2$, $\beta_{\parallel}=0.82$) and ($\xi_k=2$, $\beta_{\parallel}=0.92$). This is because the monoenergetic electrons are oscillating about their mean axial velocity such that $\Delta\beta_{\parallel}=2\mu$. As electrons lose energy to the wave, μ becomes smaller, as discussed above, and eventually vanishes when $\beta_{\perp}=0$, hence the V shape of the phase space enclosing the electrons. The width of this V-shaped region as a function of γ agrees closely with theoretical prediction based on Eqs. (2), (3), and (5), showing that these equations do describe the electron motion adequately in this example. Maximum energy loss for an electron again corresponds approximately to $\xi_k\simeq 0.6$ and $\beta_{\parallel}\simeq 0.78$. However, electron acceleration has been drastically curtailed. Maximum electron energies are only about $\xi_k=3.0$, less than half that gained without B_w.

It is possible to obtain efficiencies higher than the 11% here for conventional CARM's (uniform solenoidal field with no wiggler) by use of other operating parameters. Efficiencies in excess of 20% have been shown to be possible in semianalytic calculations with initial conditions that yield a single-particle efficiency of 100%.[6] The single-particle efficiency (the maximum efficiency an electron can achieve) may be obtained from Eq. (3) by putting $\beta_{\perp}=0$ (the figure for the above example is 70%). And in 3D wave-guide simulations, efficiencies of about 30% have been obtained.[5] Our intention in this Letter is only to point out that the use of a wiggler can significantly enhance the CARM. The maximum enhancement possible for an optimally designed conventional CARM will be explored in later studies. Also to be determined are the scalings of B_w and k_w with the operating parameters of a CARM (B_0, γ_0, $\beta_{\parallel 0}$) for optimum enhancement. Their values here were chosen by a process of trial and error. A judicious choice of B_w and k_w is necessary because if, for example, B_w is too large, the resulting large axial oscillations in the electrons' motion will prevent the resonance condition [Eq. (1)] from being satisfied by any electron, and, hence, no gain will result, while if B_w is too small, the enhance-

ment will be unattractive. As a rough measure of the sensitivity to B_w in this example, decreasing B_w by 50% reduces the efficiency of the k mode corresponding to the peak efficiency of 32% to 19%, while increasing B_w by 25% and 50% reduces the efficiency to 25% and less than 1%, respectively.

We note that this scheme is different from previous proposals for enhancement which are based on tapering the solenoidal field. One merit of it is that it does not require the development of any new technology. The helical magnetic field modeled is already in use as the wiggler in many free-electron-laser (FEL) experiments. But unlike FEL's, CARM's require the electron beam to have an initial transverse momentum, which may be effected by passing the beam through a wiggler or along a nonuniform solenoidal field. One problem has been that the high uniformity in transverse momentum and low noise level desirable for optimum operation have proved difficult to achieve. However, the enhancement in gain and efficiency that may be possible by use of a wiggler may help to alleviate the problem of achieving high beam quality and increase the attractiveness of the CARM over the FEL which typically has an efficiency of only a few percent (with a uniform wiggler).

This scheme may also have potential application in a cyclotron autoresonance particle accelerator.[7] It may be seen from Fig. 1 that selective suppression of autoresonant deceleration can be achieved by the same means as autoresonant acceleration. By choosing the initial conditions so that $k_w r_{w0} > \Omega_0/\gamma_0$ (curve 3), electrons losing energy to the wave can be made to go off resonance with the wave rapidly, hence terminating the deceleration.

This work was supported by the U.S. Air Force Office of Scientific Research under Contract No. F49620-85-K-0021, the National Science Foundation under Contract No. ECS-86-03644, and the U.S. Office of Naval Research.

[1]J. L. Hirshfield and V. L. Granastein, IEEE Trans. Microwave Theory Tech. 25, 522 (1977).

[2]V. L. Bratman, N. S. Ginzburg, G. S. Nusinovich, M. I. Petelin, and P. S. Strelker, Int. J. Electron. 51, 541 (1981).

[3]K. R. Chu and J. L. Hirshfield, Phys. Fluids 21, 461 (1978).

[4]J. L. Hirshfield, K. R. Chu, and S. Kainer, Appl. Phys. Lett. 33, 847 (1978).

[5]A. T. Lin, Int. J. Electron. 57, 1097 (1984).

[6]J. L. Vomvoridis, Int. J. Electron. 53, 555 (1982).

[7]A. Leob and L. Friedland, Phys. Rev. A 33, 1828 (1986).

[8]S. H. Gold, W. M. Black, H. P. Freund, V. L. Granatstein, R. H. Jackson, P. C. Efthimion, and A. K. Kinead, Phys. Fluids 26, 2683 (1983).

[9]A. T. Lin, J. M. Dawson, and H. Okuda, Phys. Fluids 17, 1995 (1974).

APPENDIX 4

Stability and Tunability of a CARM Amplifier

A.T. Lin and K.R. Chu*

Department of Physics

University of California at Los Angeles

and

A. Bromborsky

Harry Diamond Laboratory

Adelphi, Maryland

March 1987

*Permanent address: Department of Physics

National Tsing Hua University

Hsinchu, Taiwan, R.O.C.

ABSTRACT

Theoretical analysis and computer simulations have been carried out to examine the stability and tunability of a CARM (cyclotron auto resonance maser) amplifier. It is shown that frequency tunability over one octave can be achieved by magnetic field tuning within the stabililty range. Tunability can be further enhanced if the waveguide wall is made lossy to increase the threshold of the absolute instability. However, beam momentum spread is found to have a strong deteriorating effect on the tunability and gain.

I. Introduction

During the last two decades, there is intense interest in developing fast-wave devices based on the mechanism of electron cyclotron resonance maser. The resonant condition between an electron and an electromagnetic wave propagating in uniform magnetic field is $\omega = \Omega_c + k_z v_z$ where ω is the wave frequency $k_z v_z$ is the Doppler shift, and Ω_c is the relativistic electron cyclotron frequency. Gyrotron [1] operates in the regime where $\Omega_c >> k_z v_z$. The efficiency of a relativistic gyrotron is lower than a weakly relativistic gyrotron because in the former case a small percentage change in the electron energy will result in a large detuning of the resonant condition. In the case of a gyro-TWT (gyrotron travelling wave tube amplifier), the operating frequency is only slightly above the cutoff frequency of the waveguide and hence is very close to the oscillation frequency of the absolute instability. This makes it difficult to find a scheme to suppress the absolute instability without affecting the amplified wave.

Most of these problems can be alleviated by going into the regime where $k_z v_z$ dominates over Ω_c [3,4,]. Substituting v_{ph} ($\equiv \omega/k_z$) for k_z, the resonance condition becomes $\omega = \Omega_c/(1- v_z/v_{ph})$. Thus ω can be substantially higher than Ω_c if v_z is close to v_{ph}. It has also been shown that under the condition $v_{ph} < c^2/v_z$, the increase in Ω_c can be compensated by the decrease in $k_z v_z$ such that the resonance condition is maintained over a long interation time. This is the auto resonance conditon exploited by the CARM. In a CARM amplifier, the operating frequency is well above the cutoff frequency. When oscillation does take place near the cutoff frequency due to an absolute instability, it is relatively easy to selectively supress the absoulute instability. In addition, the oscillation can be suppressed either by injecting a signal with intensity well above the noise level [5] or by

resistively coating the waveguide wall.

In addition to the advantages of high efficiency and high frequency (relative to Ω_c), the frequency of a CARM amplifier is tunable by means of varying either the electron beam energy or magnetic field. In this paper the latter scheme is investigated through theoretical analysis and computer simulations. Instead of covering a broad data base, we will illustrate the general properties through a particular example given in Table I. The results show a frequency tunability of more than 100% over a magnetic field range of 40% (within this range the amplifier remains absolutely stable). The effects of beam momentum spread and waveguide wall resistivity are also addressed. The linear theory is presented in Section II, which is found to be in good agreement with computer simulations given in Section III.

II. Linear Theory

Brigg's criteria for absolute and convective instabilities [6] and previous linear theories of the gyro-TWT [2,7,8] have been applied to the case under study.

Fig. 1a shows the intersection of the waveguide mode and beam-wave resonance line at a grazing angle. This is typical of the gyro-TWT operation. For the CARM, it is preferable to operate at a higher magnetic field so that the upper intersecting point has a phase velocity near the speed of light. This will result in auto resonance and therefore the extraction of beam streaming energy. When the magnetic field is raised, however, the lower intersecting point will move to the left and eventually an absolute instability (oscillation) sets in as a result of backward wave excitation. Thus, for the stable operation of the CARM, there exists an upper limit on the magnetic field, which we label as B_{osc}.

When the magnetic field is above the grazing magnetic field Bg (for which the grazing intersection in Fig. 1a is realized), the approximate analytical criteria for the prediction of absolute instability derived in Ref. 2 is no longer valid. Here, we resort to the original criteria in Ref. 6 for the determination of the threshold of the absolute instability by numerically tracing the behavior of the roots of the dispersion relation [7] in the ω-k_z space. Fig. 1b plots B_{osc}/Bg as a function of a wall loss parameter δ, defined as the ratio of the wall skin depth to the wall radius. It is seen that there is a 40-60% range of stable magnetic field, depending on the wall loss. We note that $\delta = 0.01$ represents an extremely lossy wall, which can be realized only for waveguide of very small radius. A magnetic field tuning range of 40%, however, can lead to a frequency tuning range over 100%, as is shown in Fig. 2.

Also shown in Fig. 2 is the linear gain in one cutoff wavelength ($2\pi c/\omega_c$) of the waveguide for four values of axial momentum spread $\Delta p_z/p_{z0}$, where Δp_z is the standard deviation of p_z from the average value p_{z0}, assuming a Gaussian type distribution. The gain is more sensitive to the momentum spread at higher magnetic field (hence higher frequency). This is because velocity spread results in broader spread in Doppler shifts at larger propagation constant k_z. Because of its sensitivity to the velocity spread, the CARM amplifier requires a very good quality beam in order to operate in a highly Doppler shifted regime.

If wall loss is enhanced to achieve higher tunability (Fig. 1b), a fraction of the extracted beam energy will be dissipated on the wall. Fig. 3 shows that, in the preferred regime of CARM operation (high end of the stable magnetic field range), the Ohmic power loss is small as compared with the output wave power.

III. Computer Simulation Results

Particle simulation is a very powerful tool to model various free electron devices [9]. In our simulation code the transverse profile of the electromagnetic fields is fixed (TE_{01} mode) whereas the longitudinal profile and temporal evolution are self-consistently determined by integrating the Maxwell's equations using the perturbed beam current as the source. Longitudinal dependence of the fields is decomposed into Fourier components to provide resolution of the simultaneous presence of different modes. This is an essential feature for analyzing the absolute instability in a CARM amplifier. Electrons are injected at the entrance end with prescribed parameters and diagnosed at the output end. Their trajectories in the interaction region are followed through the relativistic equation of motion and the Lorentz's forces consist of the self-consistent as well as externally applied fields. Typically, thousands of electrons are used so that beam momentum spread is well represented. The fact that electrons experience inhomogeneous electromagnetic fields is included in the code by allowing electron motion in three spatial dimensions. The wall resistivity is modelled by imposing a damping term in the Maxwell's equation with a damping rate $\sigma/\omega_c = \delta/r_w$ where δ and r_w are respectively the skin depth and waveguide radius. Using the parameters in Table I, a series of simulations have been carried out to study the stability and tunability of a CARM amplifier.

Fig. 4a shows the steady state ($\omega_c t = 200$) spatial profile of the wave field for a run with $\Delta p_z/p_{zo} = 0$ and $B = 1.15B_g$. The drive power is 3.75 MW at a frequency of 2.863 ω_c. Immediately after lanunching, the wave shows no appreciable growth because of the launching loss. There is then a region of exponential growth giving a linear growth rate of approximately 3dB per cutoff wavelength, in very good agreement with the analytical prediction. Saturation

is reached at the output end where the efficiency is approximately 20%. Fig. 4b shows the electron kinetic energy versus its phase ($\phi = \omega_0 t - k_z z - \tan^{-1}\frac{p_x}{p_y}$) relative to the signal wave. The saturation is caused by phase trapping of the electrons as can be clearly seen in the phase space plot that at the exit plane where an electron bunch is formed in the decelerating phase and it is rotating in phase space. Two other simulations with B=Bg and 1.3 Bg (which are still in the stable regime according to the theoretical prediction) have been performed. The efficiencies are, respectively, 16% and 23%. The linear gains for all three cases are plotted in Fig. 3 as solid dots. To investigate the effects of beam momentum spread on the linear gain, the three cases are rerun with $\Delta p_z/p_{z0}$ increased to 0.01. The results are also shown in Fig. 3. The spread substantially reduces the linear gain, especially in the high magnetic field regime of interest to CARM. The devices become unattractrive due to low gain and low efficiency if beam momentum spread is greater than 3%.

In the case of B=Bg (gyro-TWT regime), the phase velocity of the signal wave is too far above the speed of light to satisfy the auto resonance condition. Hence, only the transverse beam energy is converted into radiation, as can be seen in Fig. 5a where the time evolution of beam transverse and longitudinal energies at the output end is shown. As the magnetic field is raised to 1.3 Bg the phase velocity of the signal wave becomes close enough to the speed of light to satisfy the auto resonance condition. This results in the conversion of both beam transverse and longitudinal energies into radiation which is clearly exhibited in Fig. 5b. The saturated efficiency therefore increases from 16% in the gyro-TWT regime to 23% in the CARM regime. According to the theory in Sec. II (Fig. 16), further increasing the magnetic field to B> 1.4Bg will bring in the absolute instability. A run with B = 1.5 Bg has been carried out to confirm this prediction. The wave

spatial profiles at two instants are shown in Fig. 6a ($\omega_c t$=100) and Fig. 6b ($\omega_c t$=200). As the absolute instability grows into long wavelength oscillation, it modulates the amplified wave and results in a reduction in output power at the desired frequency. One method of suppressing oscillations is by resistive coating of the waveguide wall. This scheme allows the device to operate at a higher magnetic field and thereby enhances the efficiency and increases the tunable range. In order to investigate these effects, a run with B = 1.5 Bg and δ = 0.08 r_w is performed and the spatial distribution of the wave field at $\omega_c t$ = 200 is displayed in Fig. 6c. The wall loss substantially but not completely suppressed the long wavelength oscillation with negligible effect on the amplified wave. The output power in Fig. bc is mainly at the input frequency. However, the required resistivity for absolute instability stabilization is almost one order of magnitude higher in simulation runs than predicted by theory.

In summary, theoretical analysis and computer simulations have been carried out to investigate the stability and tunability of a CARM amplifier. The results show that more than 100% tunability can be achieved by magnetic field tuning within the stability region. Beam quality is of critical importance to the performance of the CARM amplifier.

Acknowledgements

This work was supported by AFOSR under contract No. F49620-85-K-0021, NSF under contract No. ECS86-03644, and ONR.

References

1. J. L. Hirshfield and V. L. Granatstein, "The Electron Cyclotron Maser - An Historical Survey" IEEE Trans Microwave Theory and Techniques, Vol. MTT-25, 522 (1977).
2. Y.Y. Lau, K.R. Chu, L.R. Barnett, and V. L. Granatstein, "Gyrotron Travelling Wave Amplifier: "Analysis of Oscillatons", Int. J. Infrared And Millimeter Waves, Vol. 2, 373 (1981).
3. V.L. Bratman, N.S. Ginzburg, GS. Nusinorich, FM.I. Petelin, and P.S. Strelkov, "Relativistic Gyrotrons And Cyclotron Autoresonance Masers, "Int. J. Electron, Vol. 51, 541 (1981).
4. A.T. Lin, "Doppler Shift Dominated Cylotron Masers, "Int. J. Electron, Vol. 57, 1097 (1984).
5. A. T. Lin and Chih-Chien Lin, "Doppler-Shift Dominated Cyclotron Maser Amplifiers", Int. J. Infrared And Millimeter Waves, Vol. 5, 41 (1985).
6. R.J. Briggs, "Electron STream Interaction With Plasma", M.I.T. Press, Cambridge, M A (1964), Chapter 2.
7. K.R. Chu, A. T. Drobot, H.H. Szu, and P. Sprangle, "Theory And Simulation of the Gyrotron Travelling Wave Amplifier Operating at Cyclotron Harmonies", IEEE Trans. Microwave Theory and Techniques, Vol. MTT-28, 313 (1980).
8. Y.Y. Lau, K.R. Chu, L. Barnetta, and V.L. Grtanatstein, "Gyrotron Travelling Wave Amplifier: Effects of Velocity Spread and Wall Resistivity", Int. J. Infrared and Millimeter Waves, Vol. 2, 394 (1981).
9. M. Caplan, "The Gyrotron "An Application of the Relativistic Bunching of Electrons to the Generation of Intense Millilmeter Microwave Radiation", Ph.D. Dissertation, Dept. of Physics UCLA (1986).

Figure Captions:

Fig. 1 (a) Grazing intersection of the waveguide mode and the beam-wave resonance line. (b) B_{osc}/Bg versus the wall loss parameter δ. Parameters in Table I were used for Fig. 1b and subsequent figures.

Fig. 2 Center frequency (dashed line) and linear gain per cutoff wavelength (solid lines) versus the operating magnetic field. $\delta = 0$ is used. Gains for $\delta = 0.005$ and 0.01 are only slightly different (less than 5% lower). Simulated linear gain (dots) is in good agreement with theory.

Fig. 3 Power lost on the wall as a function of the operating magnetic field. The correrspondingoperating frequency is shown in Fig. 2.

Fig. 4 Simulation results for $B = 1.15$ Bg (a) spatial profile of the wave field at $\omega_c t = 200$. (b) electron kinetic energy versus its phase relative to the input wave.

Fig. 5 Simulated evolution of electron beam axial and transverse energies at the output enld for a) $B = Bg$, (b) $B = 1.3$ Bg.

Fig. 6 Simulated spatial profiles of the wave field for $B = 1.5$ Bg. (a) $\omega_c t = 100$. ($\delta = 0$) (b) $\omega_c t = 200$. ($\delta = 0$) (c) $\omega_c t = 200$. ($\delta = 0.08\ r_w$)

Table I. An Illustrative Example of the CARM Amplifier

Waveguide mode	TE_{01}
Electron energy	767 keV (γ_o = 2.5)
Beam current	2.5 kA
$\beta_\perp$ (= $v_\perp/c$)	0.4
α (= $v_\perp/v_z$)	0.485
Electron guiding center radius normalized to wall raduis (r_c/r_w)	0.48

(a)

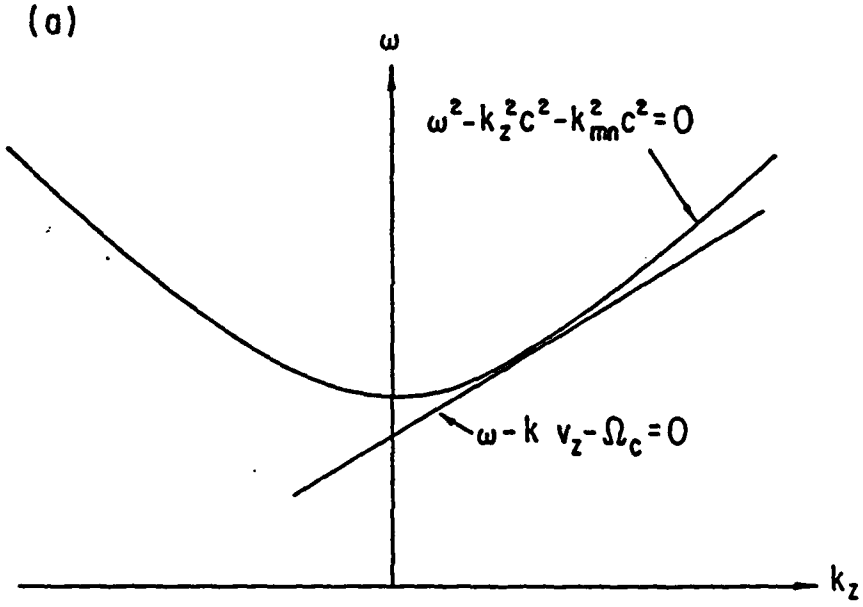
ω
$\omega^2-k_z^2c^2-k_{mn}^2c^2=0$
$\omega-k\ v_z-\Omega_c=0$
k_z

(b)

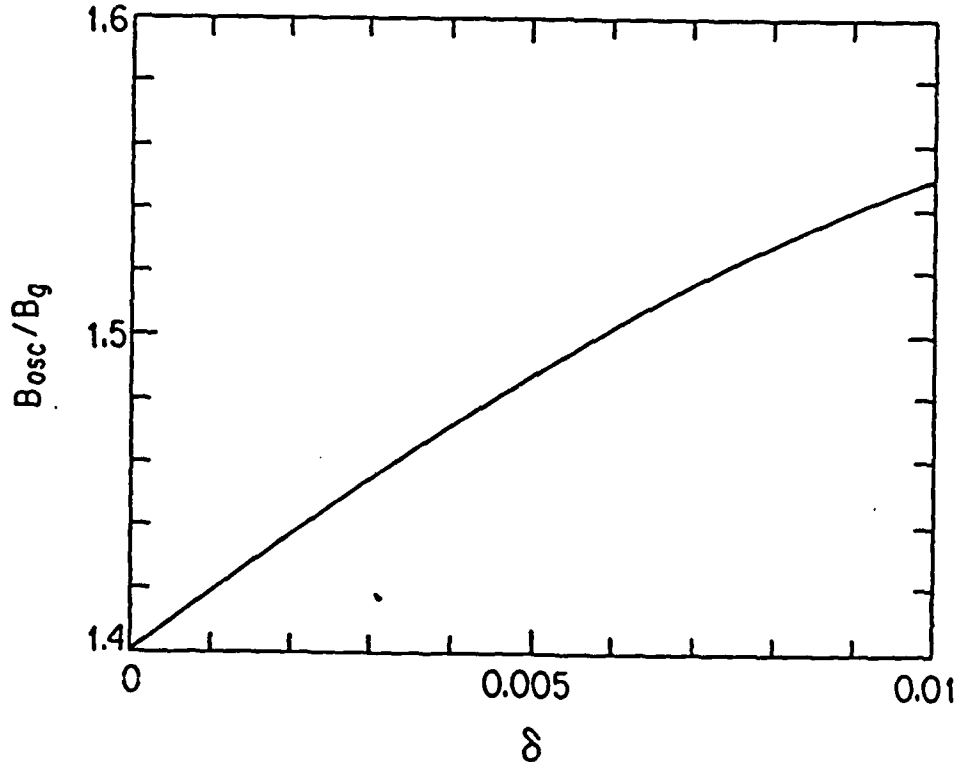
1.6
1.5
1.4
B_{osc}/B_g
0
0.005
0.01
δ

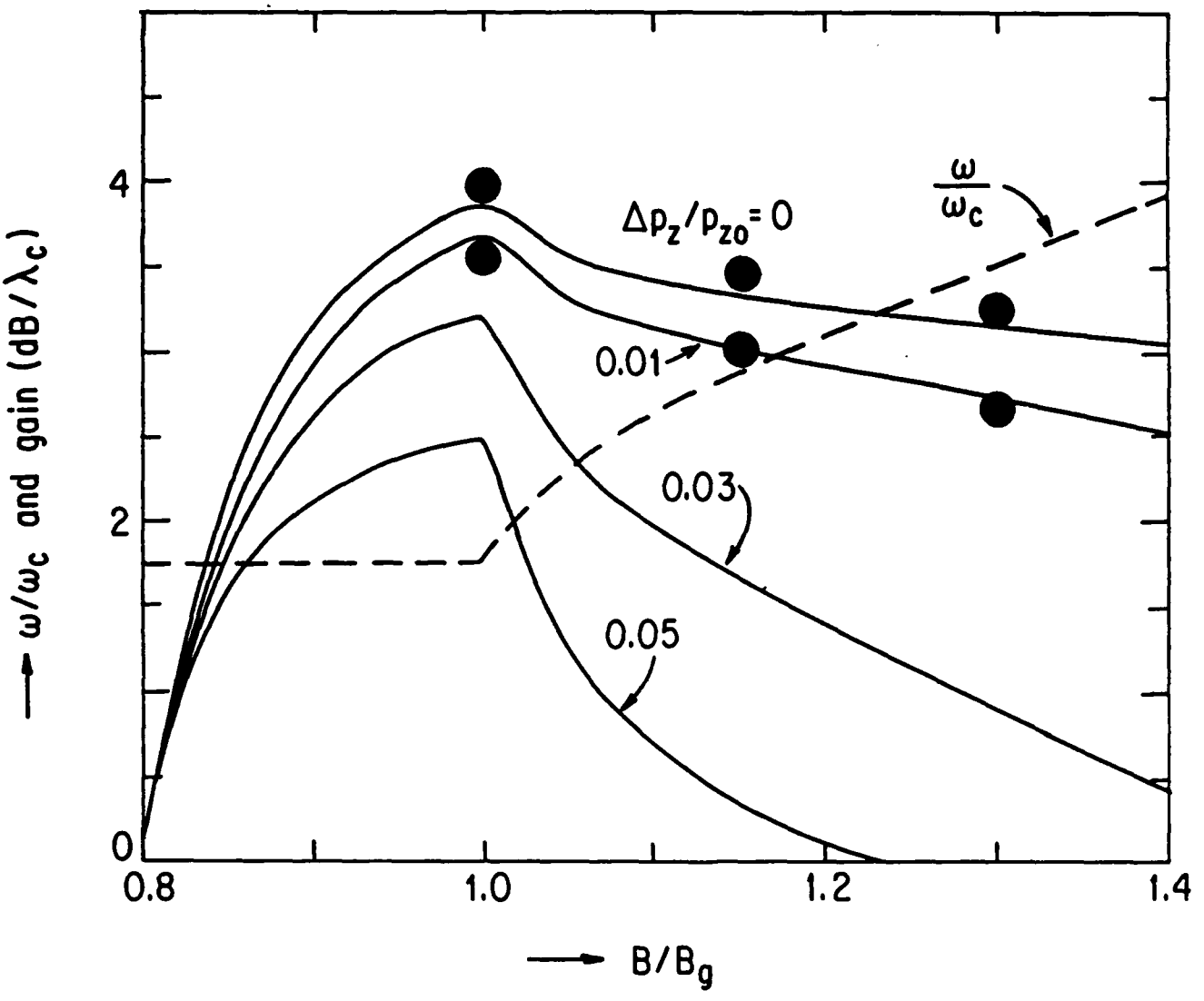
4
2
0
0.8
1.0
1.2
1.4
ω/ω_c and gain (dB/λ_c)
B/B_g
$\Delta p_z/p_{zo} = 0$
$\frac{\omega}{\omega_c}$
0.01
0.03
0.05

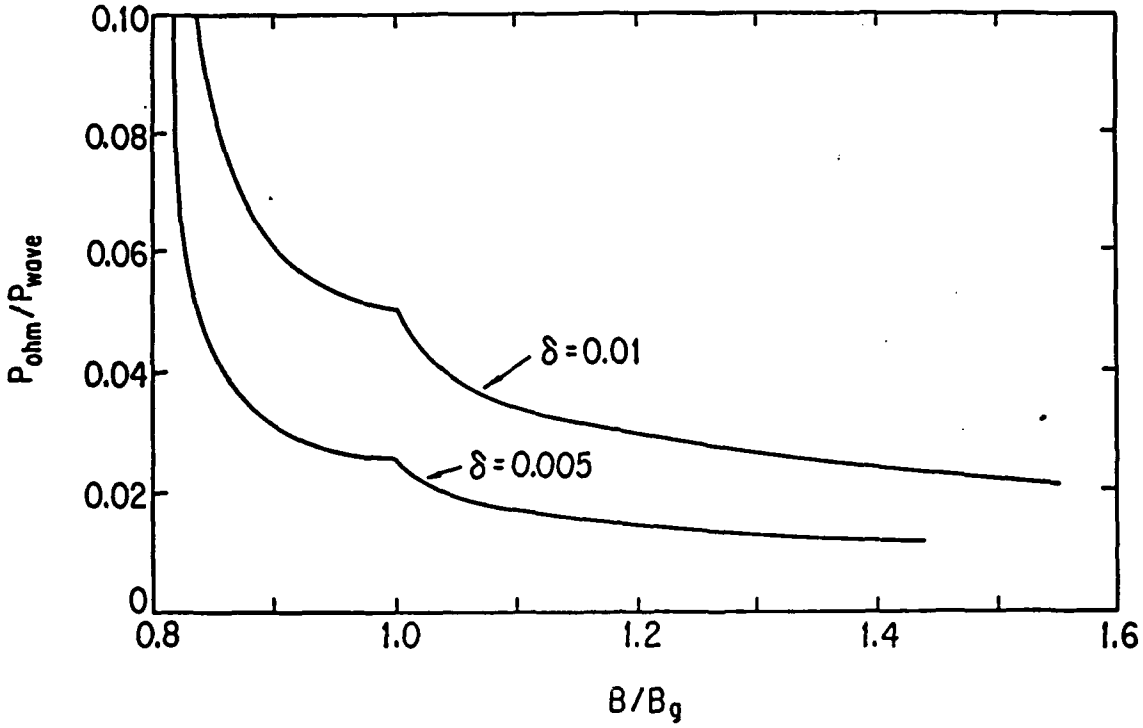
0.10
0.08
0.06
0.04
0.02
0
P_{ohm}/P_{wave}
δ = 0.01
δ = 0.005
0.8
1.0
1.2
1.4
1.6
B/B_g

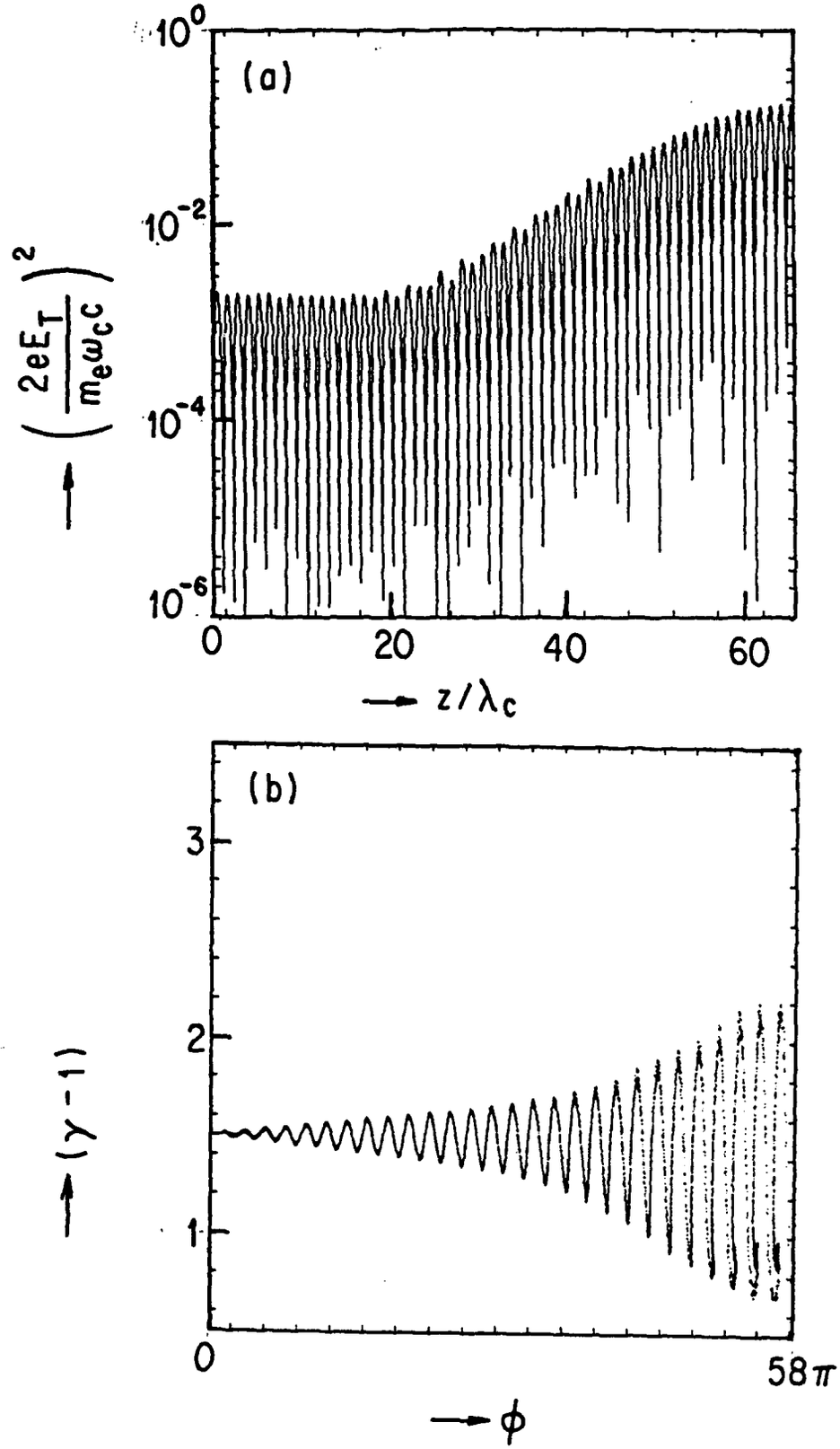
(a)
10^0
10^{-2}
10^{-4}
10^{-6}
$\left(\frac{2eE_T}{m_e\omega_c c}\right)^2$
0
20
40
60
z/λ_c
(b)
3
2
1
0
58π
$(\gamma - 1)$
ϕ

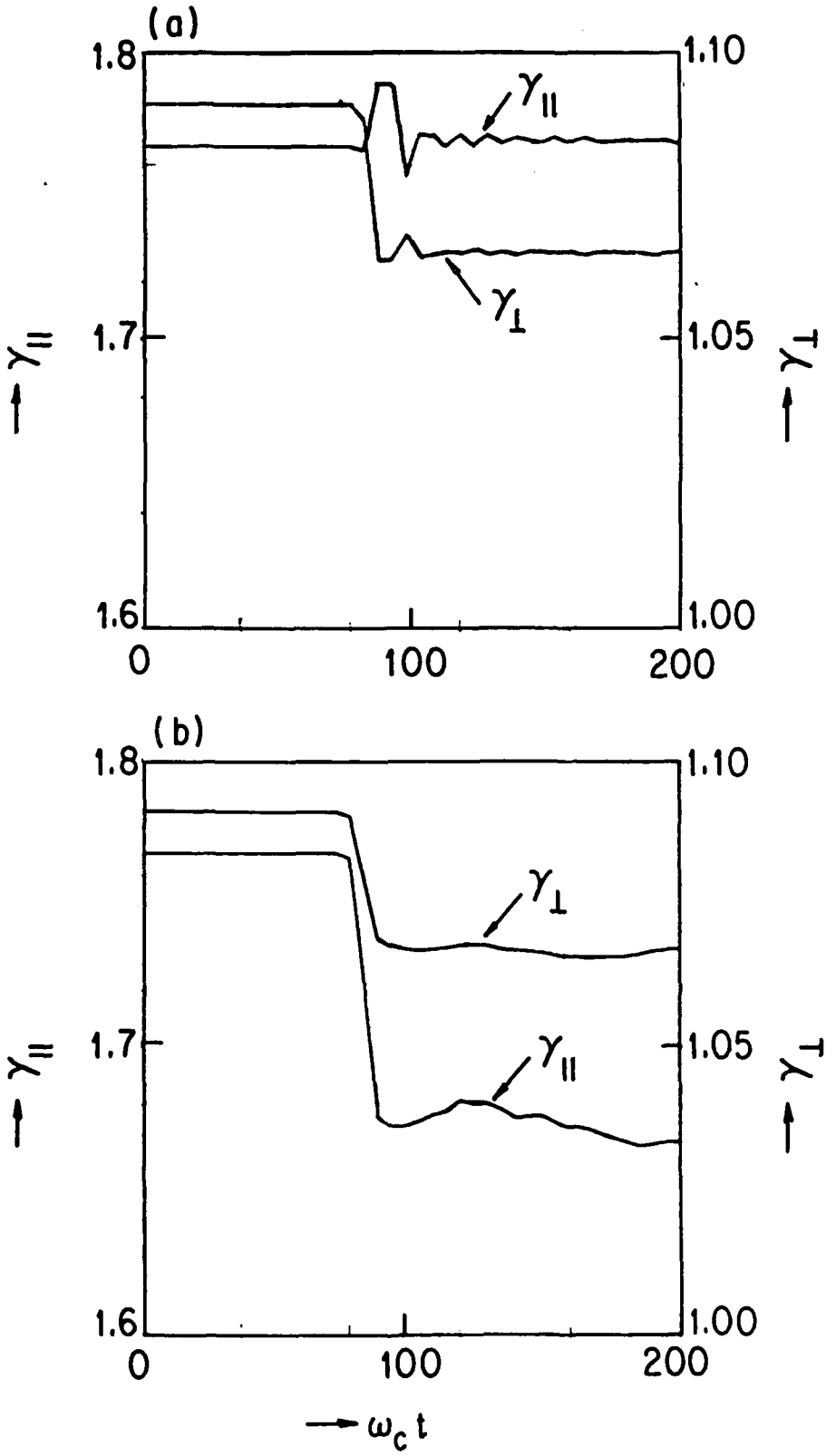
(a)
1.8
1.10
γ_{II}
$\gamma_{\perp}$
1.7
1.05
γ_{II}
$\gamma_{\perp}$
1.6
1.00
0
100
200
(b)
1.8
1.10
$\gamma_{\perp}$
γ_{II}
1.7
1.05
γ_{II}
$\gamma_{\perp}$
1.6
1.00
0
100
200
$\omega_c t$

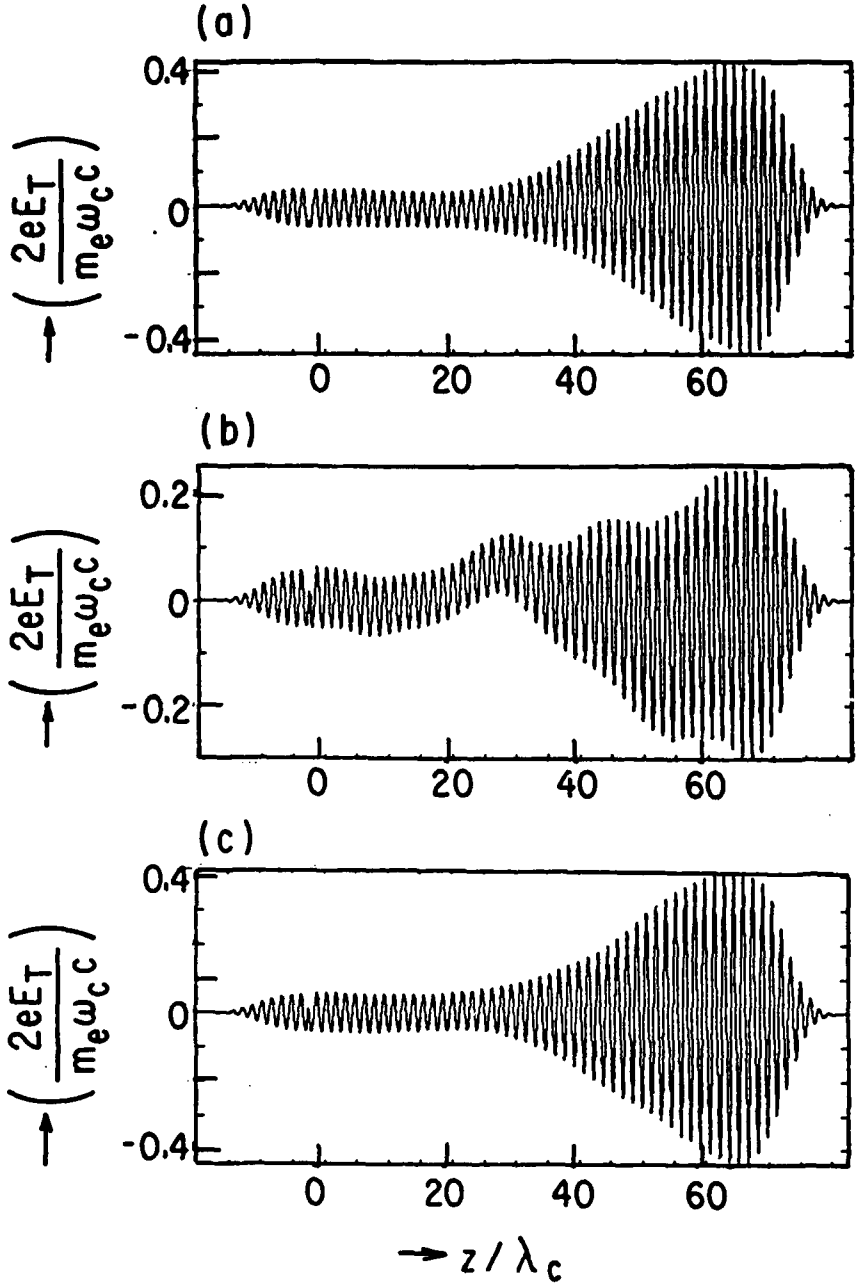
(a)
0.4
0
-0.4
$\left(\frac{2eE_T}{m_e\omega_c c}\right)$
0
20
40
60
(b)
0.2
0
-0.2
$\left(\frac{2eE_T}{m_e\omega_c c}\right)$
0
20
40
60
(c)
0.4
0
-0.4
$\left(\frac{2eE_T}{m_e\omega_c c}\right)$
0
20
40
60
z/λ_c

APPENDIX 5a

PRELIMINARY DESIGN FOR A 30 MW CARM OSCILLATOR

PHASE I

By

MALCOLM CAPLAN, JEFF NEILSON

Prepared for:

DEPARTMENT OF PHYSICS
U.C.L.A.
1 - 130 KNUDSEN HALL
LOS ANGELES, CALIFORNIA 91103

PREPARED BY:
VARIAN ASSOCIATES, INC.
MICROWAVE TUBE DIVISION
611 HANSEN WAY
PALO ALTO, CALIFORNIA 94303

Introduction:

This report describes the work done by Varian Associates on the study of the Cyclotron Auto Resonance Maser (CARM) for the contract with U.C.L.A. during the fiscal year 1986. The approach taken was to study the CARM oscillator from the point of view of designing a specific experiment, schematically illustrated in Figure 1. The design parameters chosen would allow the use of an existing 500 kV, 200 amp Magnetron Injection Gun design (with some modification) and a 28 GHz gyrotron magnet. This could allow a cost effective experiment to be performed which would be sufficient to demonstrate the CARM as a viable device and verify the basic physics.

The rest of this report is organized as follows: Section I describes how the basic design parameters where chosen. In Section II, prediction of saturated output power and efficiencies are presented indicating regions of hard and soft excitation. Section III gives preliminary designs for the magnetron Injection Gun and Bragg Reflector. Finally, Section IV discusses the future work required to improve and fully verify the final design.

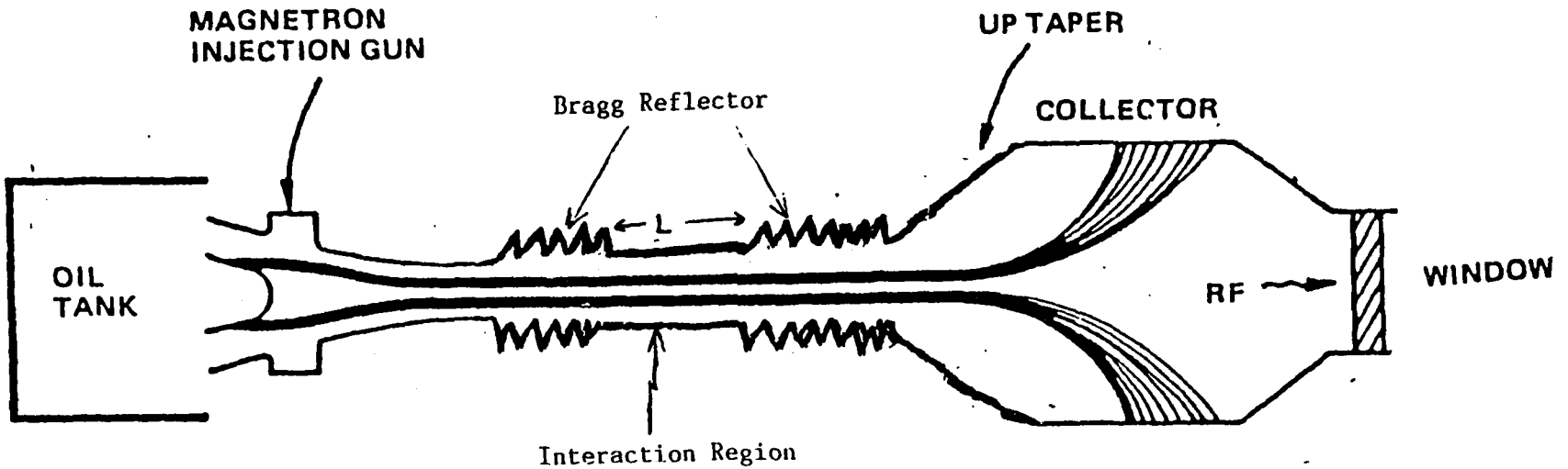

FIGURE 1 SCHEMATIC OF TE_{01} CARM OSCILLATOR

Section I. Design Considerations

The beam voltage and current were chosen to be 500 kV and 200 amps respectively in order to make use of an existing gyroklystron gun design. The cutoff frequency of the resonator section was kept at 10 GHz in order to keep the final beam guiding center the same as in the gyroklystron. This also required staying with the TE_{01} mode. The cyclotron frequency and operating frequency were determined from the conditions for cyclotron resonance and ideal cavity resonance according to the following formula:

$$\frac{\omega}{\Omega_c} = \frac{1}{1 - v_z/v_{ph}}$$

$$\frac{\omega}{\omega_c} = \frac{1}{\sqrt{1 - c^2/v_{ph}^2}}$$

where v_{ph} and v_z are the phase velocity and axial beam velocity. Previous work done at U.C.L.A. served as a guide in choosing a phase velocity of 2.69% above the speed of light in order to allow a reasonable compromise between gain and efficiency. This implied an operating frequency of 44 GHz. The transverse velocity c was chosen slightly greater than $1/\gamma$ (enhanced gain) resulting in a ratio of perpendiclar to parallel velocity (α) of .8. This resulted in a ratio of cyclotron frequency to operating frequency of $\sim 1/3$ translating into a required axial magnetic field of 10300 gauss. The cavity interaction length was determined by calculating oscillation threshold currents. The calculation was done assuming the fields were of an ideal cavity resonator whose length was N half wavelength long. This was considered for now to be a reasonable approximation to the true open resonator which would be formed from Bragg reflectors. The cavity Q was

assumed to be 500. The results shown in Figure 2 indicated that lengths greater than 50 half wavelengths would be required in order to allow start oscillation currents of less than 200 amps. An optimal design with a length of 80 half wavelengths and a Q of 650 was finally chosen although much of the following analysis was done with a cavity length of 70 half wavelengths and a Q of 600. A summary of the basic design parameters is shown in Table I.

Section II. Predictions of Saturated Output Power and Efficiency

The efficiency analysis was performed using a simplified semi-analytical model which assumed that the saturated steady state longitudinal mode structure was determined by geometry only and not greatly perturbed by the presence of the beam. A single equation for the self-consistent peak field amplitude was then determined by involving energy balance: i.e., the kinetic energy lost by electrons transversing the cavity is equal to the microwave power emitted from the cavity. The trajectories of a set of test electrons initially distributed randomly with respect to their phase angle in velocity space were integrated numerically across the cavity in the presence of the electromagnetic field to determine the average fraction of kinetic energy lost to the field for a given peak electric field amplitude. A nonlinear efficiency function was constructed which gave the fraction of beam energy converted to microwaves as a function of peak electric field $|E_o|$, magnetic field B, beam voltage V_o, ratio of perpendiclar to parallel velocity(α) and both cavity and beam geometric factors. The microwave power generated by the beam P_B was given by the following expression:

$$P_B = \eta(|E_o|^2, B, V_o, \alpha, \xi) I_o V_o$$

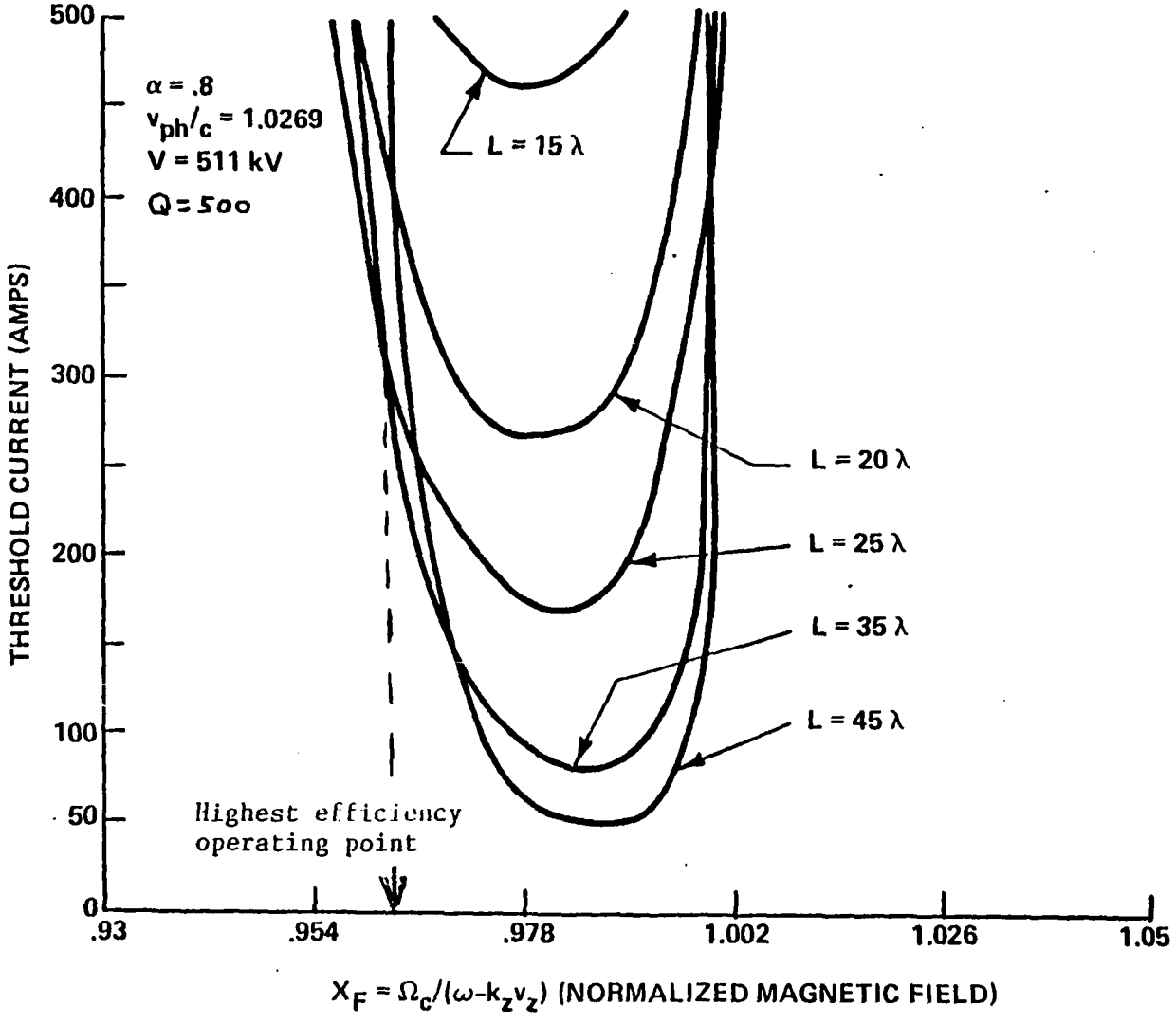

FIGURE 2 THRESHOLD CURRENT VERSUS MAGNETIC FIELD FOR DIFFERENT INTERACTION LENGTHS

TABLE I

PARAMETERS FOR CARM OSCILLATOR DESIGN

Beam Power	100 MW
Beam Voltage	511 kV
Beam α	.8
Microwave Power	$\sim$30 MW
Cavity Mode	TE_{01}
Operating Frequency	44 GHz
Cavity Cutoff Frequency	10 GHz
Cavity Interaction Length	40 wavelengths
Cavity Q	$\sim$650
Circuit Magnetic Field	10300 gauss

The power radiating from the cavity as a result of the external diffraction Q was given by:

$$P_R = \frac{\omega_o^2 \text{ (stored energy)}}{Q_D} = \text{kloss } |E_o|^2$$

where kloss is given by:

$$\text{kloss} = \left[\frac{J_m^2(k_{mn})(1 - m^2/k_{mn}^2)a_o^2\omega_R}{8Q_D}\right] \int_{z_{in}}^{z_{out}} |\bar{E}(z)|^2 dz$$

Since in steady state $P_R = P_B$, the following non-linear equation for $|E_o|$ was obtained:

$$\eta(|E_o|^2, B, V_o, \alpha, \xi)V_o I_o = \text{kloss } |E_o|^2$$

In practice, the current I_o was determined as a function of $|E_o|^2$.

Figure 3 shows efficiency versus distance for an optimal electric and magnetic field setting indicating that over 35% efficiency could be achieved. The higher electric field was optimal for a shorter length resonator. Anticipating that non-ideal beams with velocity spread would interact more efficiently in shorter resonators, a detailed efficiency analysis was performed for a cavity 35 wavelengths long. Figure 4 shows power out versus field amplitude squared assuming 200 amps of current for two different magnetic fields.

The intersection with the diffraction Q line indicates the actual operating points. One observes that the magnetic field showing higher efficiency (dotted curve) has two solutions. The lower power solution is not physical in that the system is unstable at ths point. The stable high power solution would appear inaccessible from noise (hard excitation) in that as $E \to o$, the cavity losses are greater than the power generated by the beam. Accessibility is achieved if Q is increased sufficiently to allow the Q line to have a smaller slope at the origin than the power curve. For this

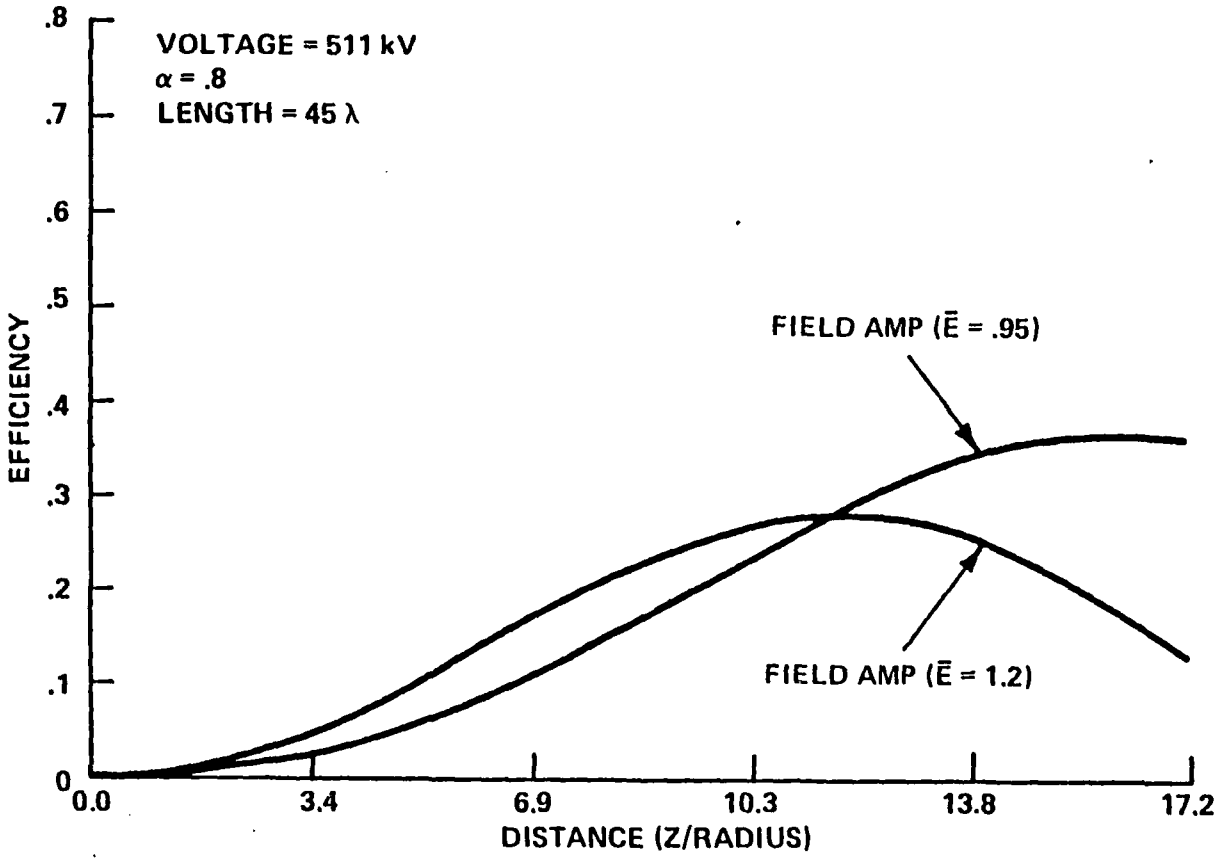

FIGURE 3 EFFICIENCY VERSUS DISTANCE Z FOR OPTIMAL AND NON-OPTIMAL ELECTRIC FIELD AMPLITUDES

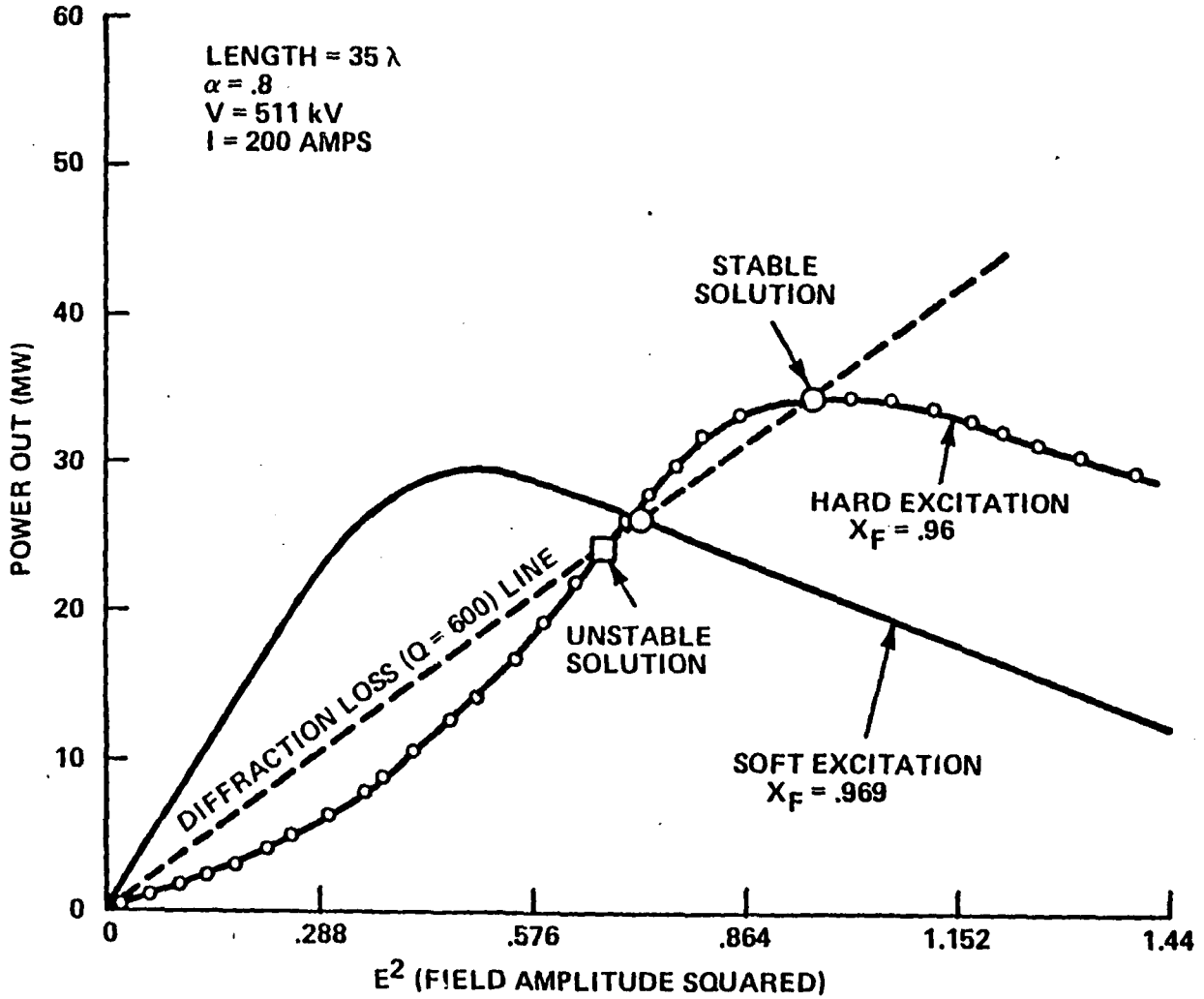

FIGURE 4 POWER OUT VERSUS FIELD AMPLITUDE SQUARED (HARD AND SOFT EXCITATION)

increased Q value, there is a single operating point intersection but at a reduced power level. In practice, the finite rise time characteristic of the beam could allow accessibility to the higher power states without changing the Q factor. This requires further investigation.. Figure 5 shows efficiency versus current for different magnetic fields: The dashed lines are the non-physical solutions. An efficiency of 34% is indicated at 200 amps resulting in a predicted output power of 34 MW. The optimum output power of 40 MW is illustrated in Figure 6, where a 3.0% magnetic taper was applied and the interaction length was increased to 40 wavelengths.

Section III. Preliminary Designs for the Magnetron Injectin Gun and Bragg Reflector

A preliminary design for the required MIG is shown in Figure 7. The initial gun was designed for an α of 1.5 at a final magnetic field of 5600 gauss. It is required to operate the gun in a final field of 10300 gauss with an α of .8 and at the same guiding center. This requires that the cathode radius be changed from 2.28 cm to 3. cm and the cathode magnetic field be increased to 845 gauss. Further, refinements of the electrode structure would be required to ensure beam velocity spreads of $\leq$2%. Table II shows the design parameters of the modified gun.

Finally, the design of the Bragg reflector is required which gives a Q of 600. In a single mode analysis one solves the following differential equation for the complex field profile E and complex ω:

$$\frac{d^2E(z)}{dz^2} + \left[\frac{\omega^2 - \omega^2_{cE}(z)}{c^2}\right] E(z) = 0$$

where:

$$\omega^2_{cE}(z) = \omega^2_c(z)\left[1 - m^2 W_L(z)/k^2_{mn}\right] \equiv \text{effective cutoff frequency}$$

$$\omega^2_c(a) = c^2 k^2_{mn}/a^2(z) \equiv \text{local cutoff frequency}$$

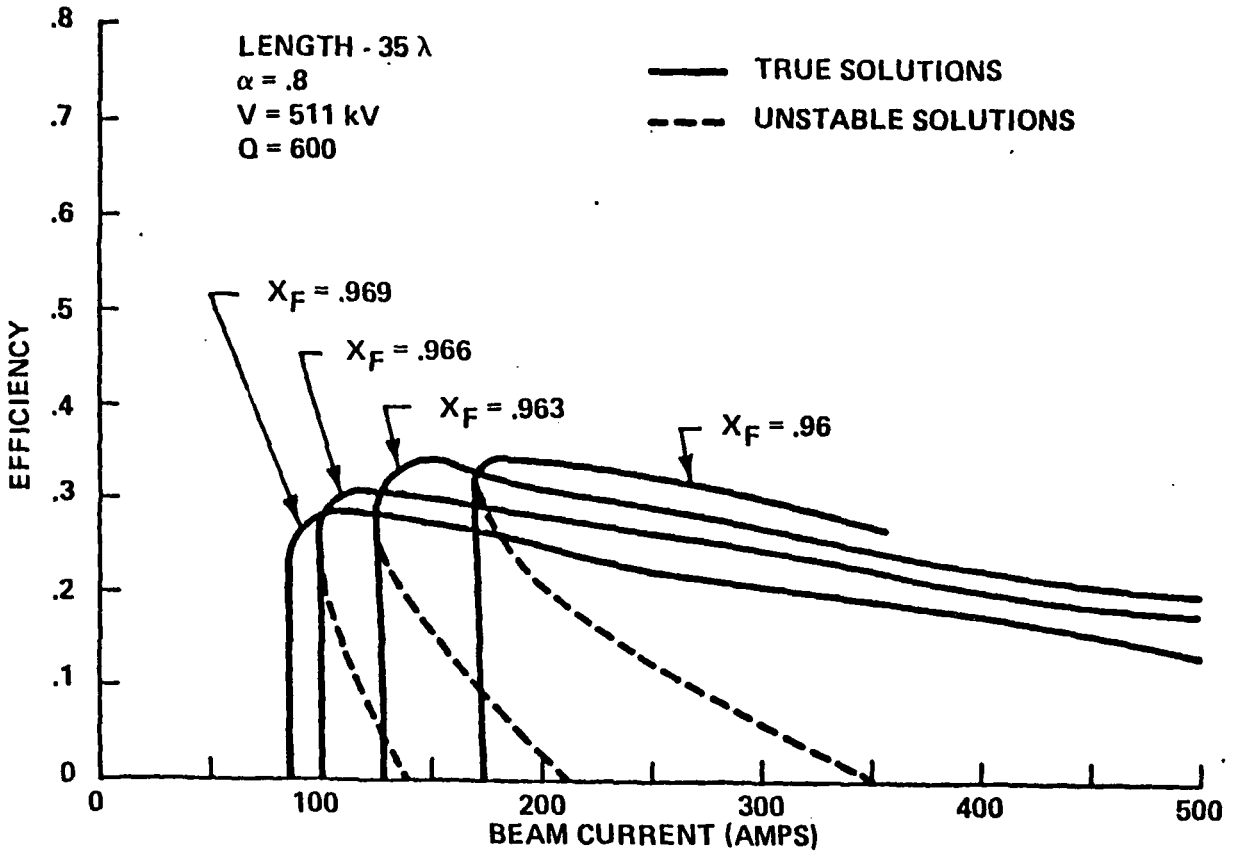

FIGURE 5 EFFICIENCY VERSUS CURRENT FOR DIFFERENT MAGNETIC FIELDS

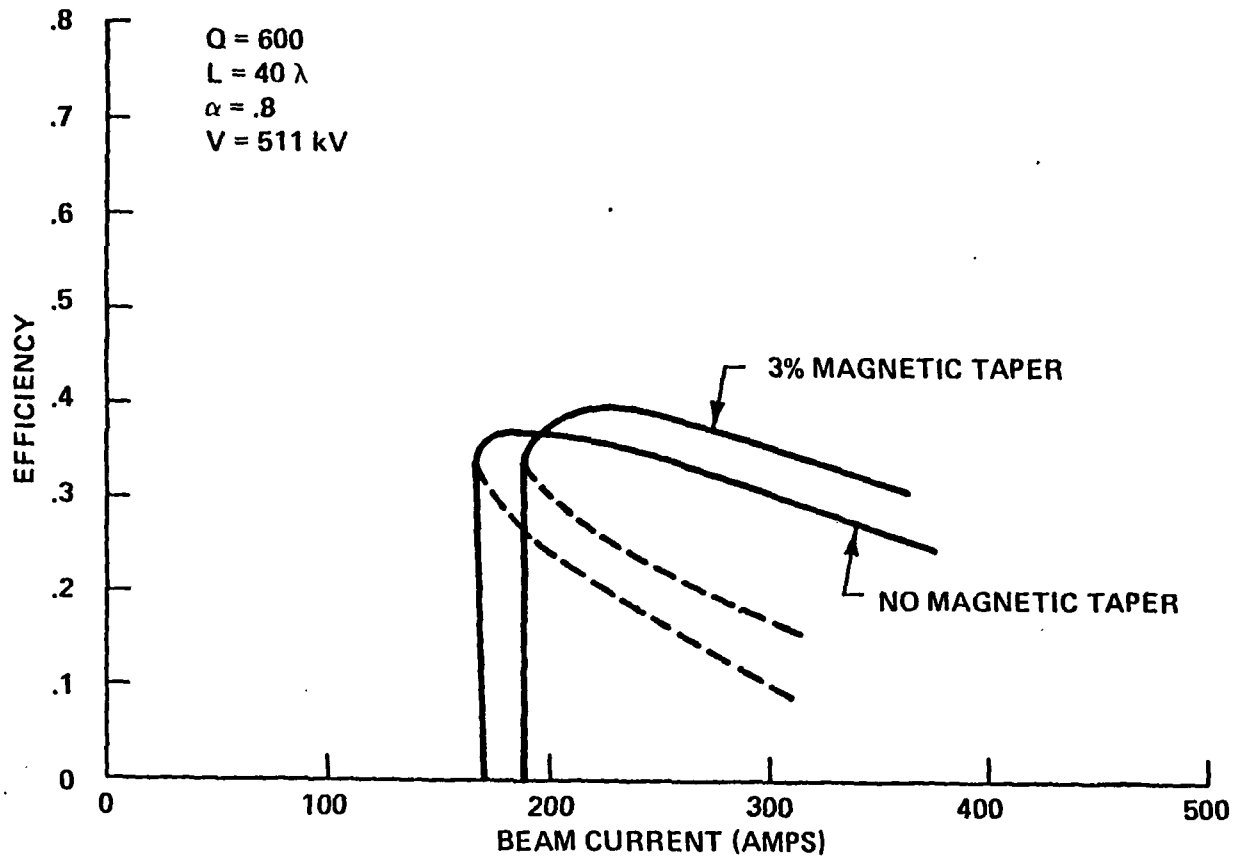

FIGURE 6 EFFECTS OF MAGNETIC TAPER ON EFFICIENCY

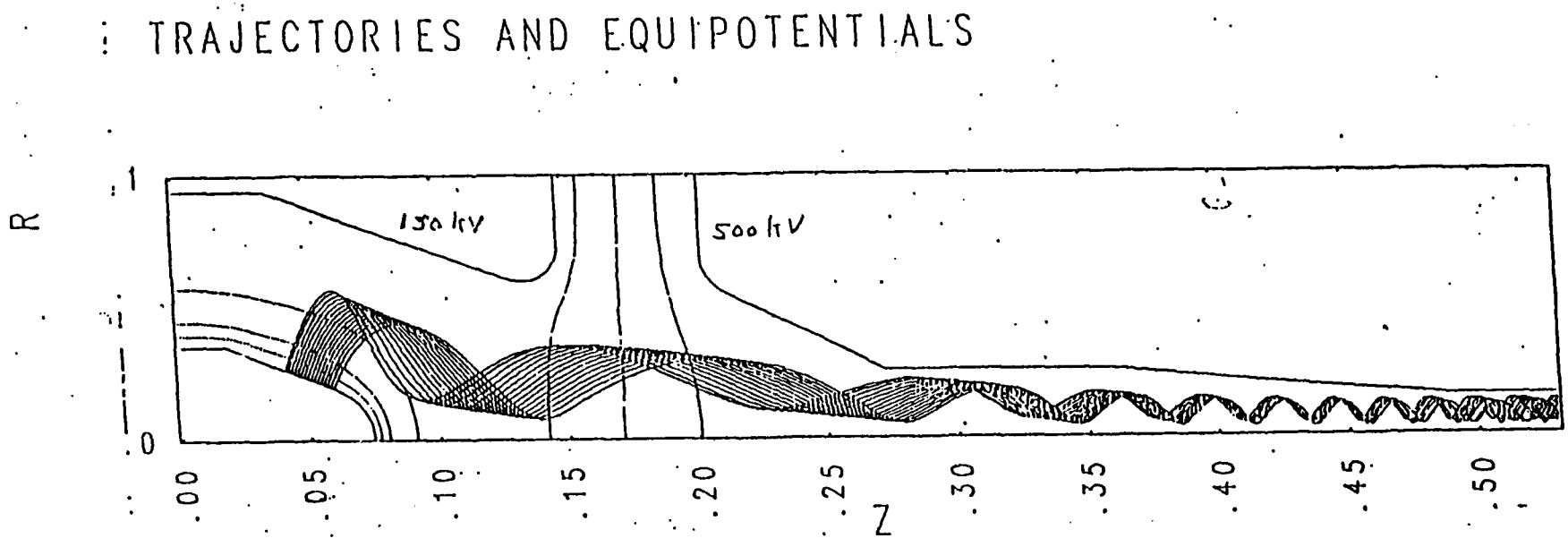

	Present Gun	New Gun
Cathode Radius	2.28 cm	3.0 cm
Cathode B Field	470 gauss	845 gauss
Final B Field	5600 gauss	10300 gauss
$V_\perp / V_{11}$ (α)	1.5	.8

FIGURE 7 PRESENT 500 kV 200 Amp MIG GUN TO BE MODIFIED FOR CARM

TABLE II

GUN PARAMETERS FOR CARM

Beam Voltage	500	kV
Anode Voltage	150	kV
Beam Current	200	Amps
Final Guiding Center	.877	cm
Final Larmor Radius	.1775	cm
Final B_L	.541	cm
Final B_Z	.676	cm
Radius Cathode	3.0	cm
Radius Anode	5.57	cm
Axial B-Field	10300	gauss
Cathode B Field	845	gauss
Beam Current/Space Charge Current	30	%
Field Gradients at Cathode	80	kV/cm

The diffraction Q of the cavity is then given by:

$$Q = \omega_R / 2\omega_I$$

An approximate expression for the frequency and Q is given by:

$$\omega_R = \sqrt{\omega_c^2 + (l\pi/L)^2} \quad \text{(Fig 1)}$$

$$Q = \frac{\omega_R L/c}{(1 - R_1 R_2)}$$

where R_1 and R_2 are the reflection co-efficient of the Bragg Reflectors. Reflection is obtained by coherent scattering of a forward wave into a backward wave which occurs when the ripple wave length is 1/2 the guide wavelength.

The mode structure of Bragg resonators (cutoff on the left side) with Q factors of 566 and 832 are illustrated in Figures 8 and 9. The real and imaginary parts (dotted line) of the field profile is indicated. Physically, the imaginary part is the field profile 90° in phase from the real part.

A more comprehensive technique for evaluating Bragg resonators is in progress using scattering matrix theory which includes all TE and TM modes capable of coupling with the rippled wall. The Bragg reflectors are characterized by scattering matrices $[S^1]$ and $[S^2]$ which describe the reflected amplitudes of a set of modes incident on the reflector. The eigenfrequency and Q are determined from the following determinant:

$$\text{Det} \quad \left\| I - [S^1]\,[S^2] \right\| = 0$$

The requirements on the Bragg reflector necessary to maintain mode purity can be determined.

Section IV. Future Work

The previous work must be thought of as a preliminary analysis. Test particle simulation must be done in the actual resonator fields indicated

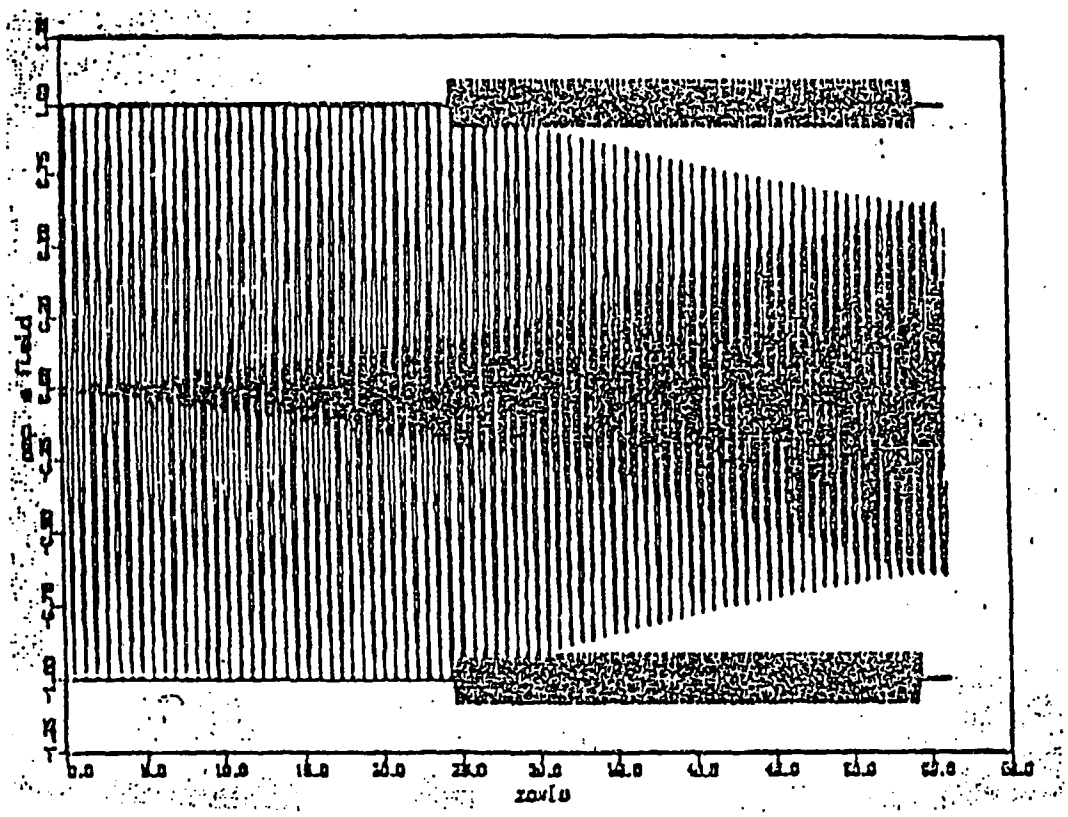

Q = 566	Length Straight Section	= 70 λ_B
f= 43.93 GHz	Length Bragg Reflector	= 85 λ_B
	Ripple Amplitude a_1/a_o	= .082

FIGURE 8 BRAGG RESONATOR FIELD PROFILE

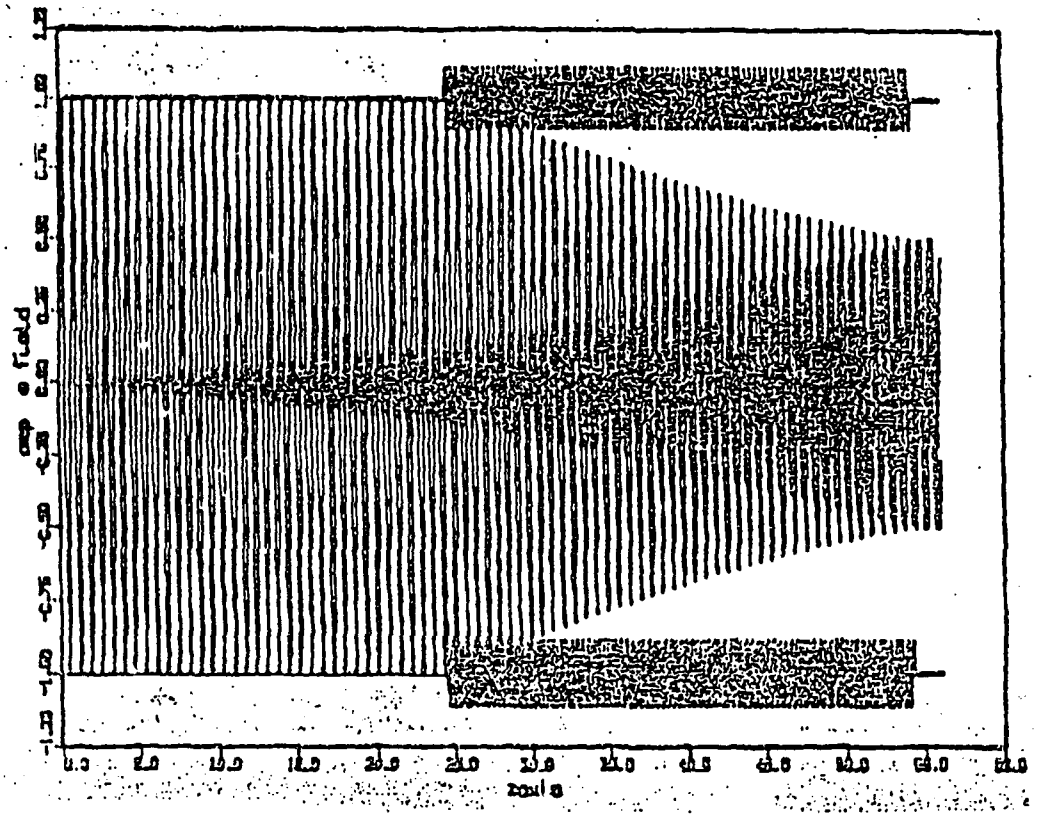

Q = 832	Length Straight Section	= 70 λ_B
f = 43.9 GHz	Length Bragg Reflector	= 85 λ_B
	Ripple amplitude a_1/a_0	= .11

FIGURE 9 BRAGG RESONATOR FIELD PROFILE

in Figure 8 and 9. Velocity spreads must be given to the initial particle distributions to evaluate the effect of beam emittance. Threshold current analysis must be done for competing modes especially the "gyrotron modes" near cutoff. Finally, a fully self-consistent EM particle simulation including space charge effects is required to verify a final design.

APPENDIX 5b

CARM OSCILLATOR STUDY

A study was undertaken to design and analyze a CARM oscillator which could operate at 150 GHz with power levels in the megawatt range. The voltage was chosen to be 400 kv in order to be compatable with possible cw applications as well as minimizing power supply requirements. The mode of operation chosen was the circularly polarized TE_{11} implying a Pierce/Wiggler configuration for beam formation, Beam quality requirements (velocity spread) limited gun pervience to $\lesssim .2$ or beam current ≤ 50 amperes. In order to be near autoresonance, the phase velocity was chosen to be 2% above the speed of light. The operation frequency of 150 GHz was thus ~ 5 times above cutoff (29 GHz). The voltage restriction of 400 kv required that the relativistic cyclotron frequency be two times the cutoff frequency (i.e., magnetic field $\sim$ 37000 gauss). An interaction diagram is shown in figure 1.

The upper intersection point is the CARM while the lower intersection point represents a possible backward wave oscillation at 43.0 GHz ($\sim$ 42% above cutoff). In order to create a standing wave in a guide far above cutoff, one uses a Bragg reflector. The resonator selects out the axial mode whose wavelength is double the Bragg ripple length. The cavity Q is in general much lower for all other resonant wavelengths (frequencies) including the mode near cutoff (ℓ=1). This is illustrated in figures 2a and 2b. A cavity was chosen with a 5 cm interaction length (25 wavelengths) and a Bragg reflector consisting of 20 ripples each having an amplitude of .014 cm. The operating mode at 150 GHz then had an effective ℓ number of 50 and an external Q of 843. The ℓ=1 mode near cutoff had a Q of 214. The main problem with this configuration is that there could be mode competition with the backward wave oscillation

which does not require external reflection to exist (very low Q).

Three different computer models were developed to analyze this oscillator configuration. The first model looks at the CARM interaction only. It assumes that only a single mode at a single frequency exists, namely the resonant mode created by the Bragg reflector. It assumes that the beam does not modify the empty cavity field profile. Electrons are integrated both analytically and numerically through these fields to obtain the start oscillation currents and saturated efficiencies respectively. The second model was developed to look at interaction with the backward wave oscillation only. This self-consintant simulation model is based on the slow time scale orbit equations coupled to Maxwell's equations. An efficient searching scheme is used to find the unknown initial magnetic field and oscillation frequency which allows the boundary conditions to be satisfied. Finally a third model has been developed which is a fully time dependent particle mode which can model self-consistently both the CARM interaction and backward wave interaction simultaneously. The code couples the exact time dependent orbit equations (represented by $X_p(t), V_p(t)$) with the following reduced set of Maxwell's equations for interaction with TE_{mn} modes:

$$\frac{\partial B^i_{Tmn}}{\partial t} = - c \frac{\partial E^i_{Tmn}}{\partial z} - cE^i_{Tmn} \frac{a'(z)}{a(z)} \left(\frac{m^2}{k^2_{mn} - m^2} \right) +$$

$$c \frac{a'(z)}{a(z)} \sum_{\ell \pm n} K_{mn\ell} E^i_{T m\ell} \frac{(1-m^2/k^2_{m\ell})}{(1-m^2/k^2_{mn})} \qquad i=1,2$$

$$\frac{\partial B^i_{Lmn}}{\partial t} = - \omega_{cmn}(z) E^i_{Tmn} \qquad i=1,2$$

$$\frac{\partial E^i_{Tmn}}{\partial t} = - c \frac{\partial B^i_{Tmn}}{\partial z} + \omega_{cmn}(z) B^i_{Lmn} + cB^i_{Tmn} \frac{a'(z)}{a(z)} \left(\frac{m^2}{k^2_{mn} - m^2} \right) +$$

$$c \frac{a'(z)}{a(z)} \sum_{\ell \neq n} K_{mn\ell} B^i_{Tm\ell} -$$

$$\frac{2L_p}{N_p} \left(\frac{\omega_B}{\omega_{co}} \right)^2 \frac{a_o}{U_{mn} a(z)} \cdot \sum_p \left[v_{xp} e^i_{xmn}(x_p, y_p) + v_{yp} e^i_{ymn}(x_p, y_p) \right] F(z - z_p)$$

$$i = 1, 2$$

where the coupling coefficient $K_{mn\ell}$ is given by:

$$K_{mn\ell} = \frac{2k_{mn} k_{m\ell} J_m(k_{m\ell})}{(k^2_{m\ell} - k^2_{mn}) J_m(k_{mn})} \cdot \left[\frac{\left| J_{m-1}(k_{mn} R_{mn}/a_o) \right| + \left| J_{m+1}(k_{mn} R_{mn}/a_o) \right|}{\left| J_{m-1}(k_{m\ell} R_{m\ell}/a_o) \right| + \left| J_{m+1}(k_{m\ell} R_{m\ell}/a_o) \right|} \right]$$

The terms proportional to m^2 model the effect of the Bragg ripples on the radial electric field which causes most of the reflection in a guide far above cutoff. Also included are mode conversion terms due to the finite size ripples.

Figure 3 shows start oscillation current versus magnetic field for the $\ell = 50$ mode. The external Q was 376 in this case (12 ripple reflector). The modes $\ell = 49$ and $\ell = 51$ shifted by ~ 2 GHz are also shown. The bandwidth of the Bragg resonator was relatively large in that the Q dropped only to 330 from 376. There is still a range of magnetic field for which only $\ell = 50$ oscillates. The discrimination between modes could be much higher for a narrower bandwidth reflector (20 ripples). However, the larger bandwidth allows the device to be tunable by varying magnetic field. Figure 4 shows a plot of efficiency versus current for two different

magnetic fields. One predicts efficiencies of 21% which results in 2MW output power for a 25 amp beam.

Figure 5a shows the self-consistent field amplitude profile for a backward wave oscillation which exists at 43 GHz. This profile is composed of a backward wave with a cosine profile mixed with a non-interacting constant amplitude forward wave produced when the wave bounces off the back wall. The efficiency is 4½%. Figure 5b shows backward wave efficiency versus length indicating a threshold length of 4.5 cm. for currents of 25 amperes. The fact that the CARM efficiency is 21% while the backward wave efficiency is ~4% suggests that the CARM will dominate. The problem could be solved by lowering the beam power (and output power) so that the threshold length for backward oscillation increases to 6 - 7 cm (i.e. greater than the CARM interaction length).

The fully time dependent code is being used now to verify the conditions under which the backward wave is suppressed and to indicate when the Bragg reflector causes excessive spurious mode conversion. These studies are in progress at this time. In summary, the following is a tentative design for a CARM oscillator based on the above analysis:

voltage	400 kv
current	25 amps
V_T/Vz	.92
frequency	150 GHz
power	2 MW
cavity Q	376
cavity length	5.1 cm
cavity radius	.29 cm
axial magnetic field	37000 gauss
beam fill factor	40%

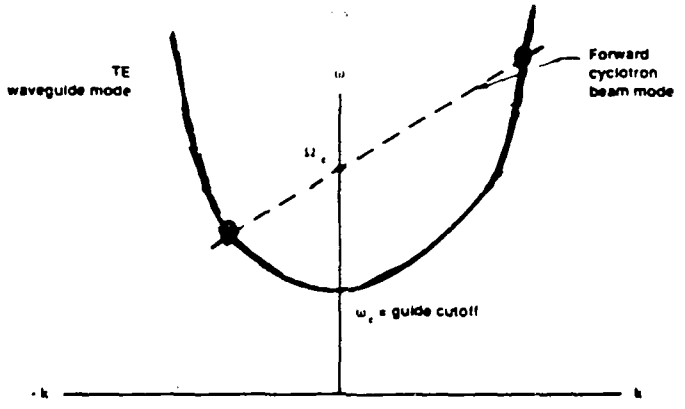

Figure 1 Interaction mechanism for CARM and backward wave oscillation

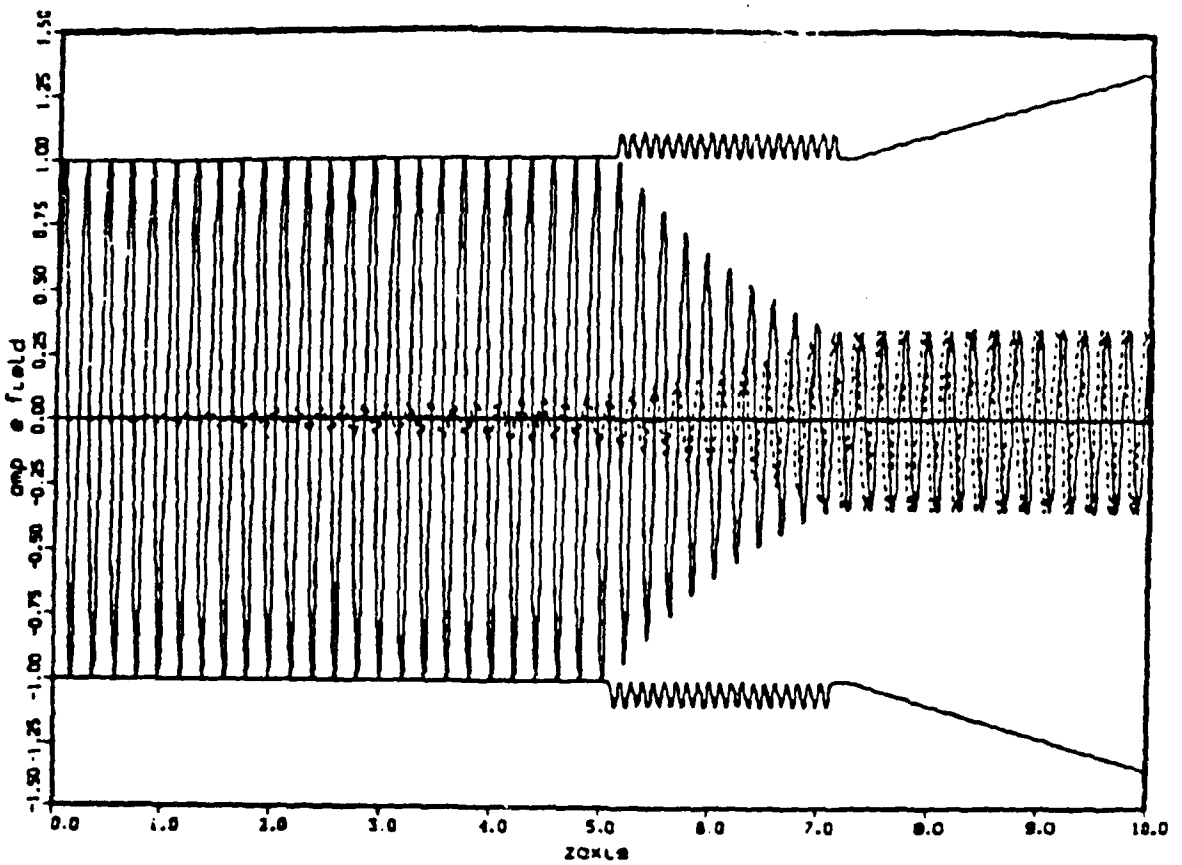

Figure 2a Operating mode Q = 848. Frequency = 150 GHz $\ell = 50$

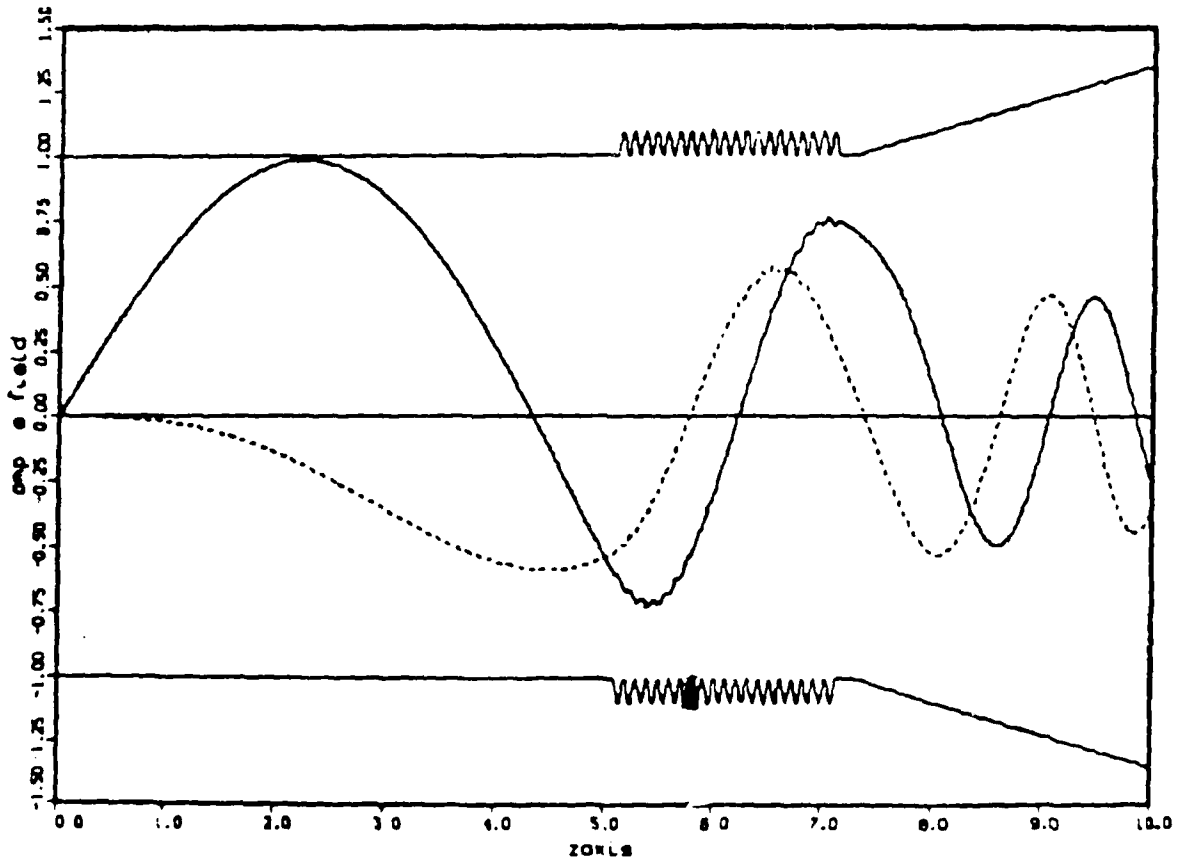

Figure 2b. Mode near cutoff. $\ell = 1$. Frequency = 29.86 GHz. Q = 214

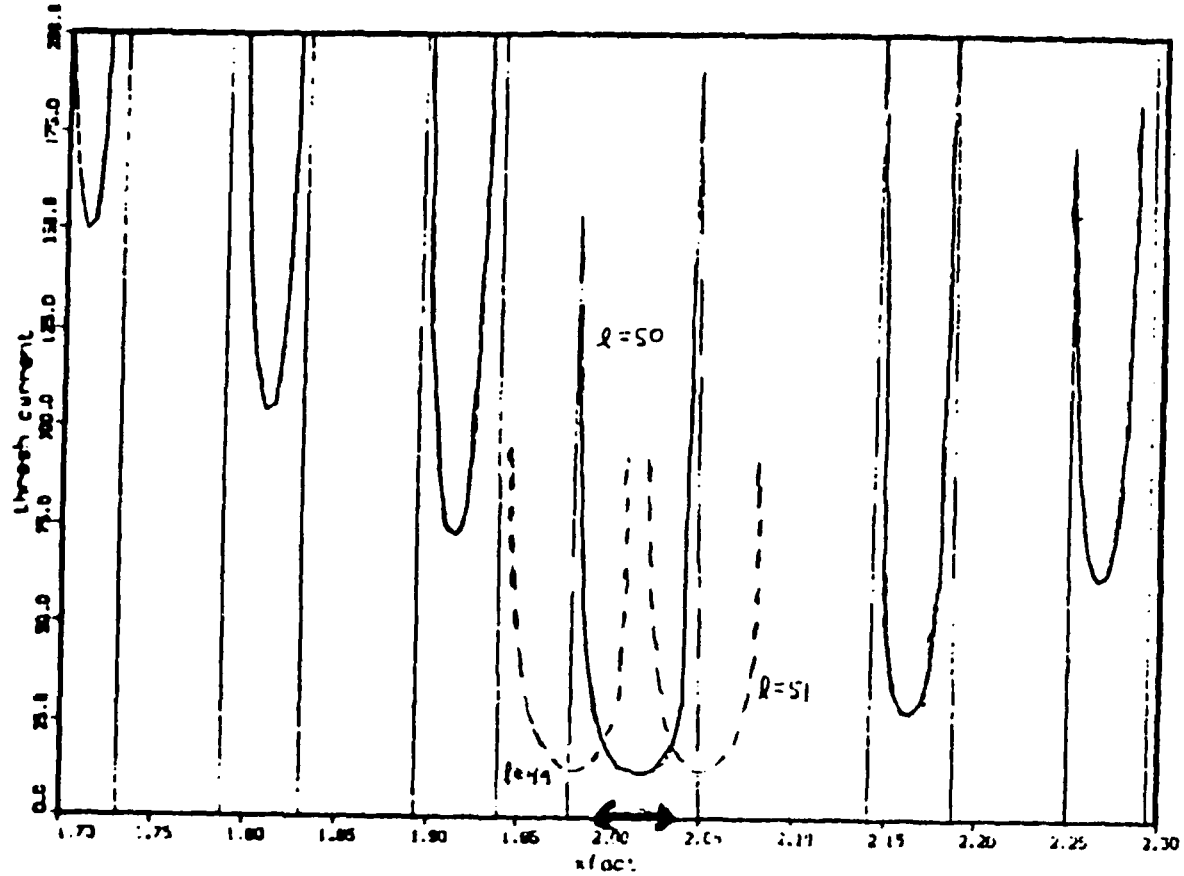

Figure 3 Start oscillation current versus magnetic field. $Q = 376$.

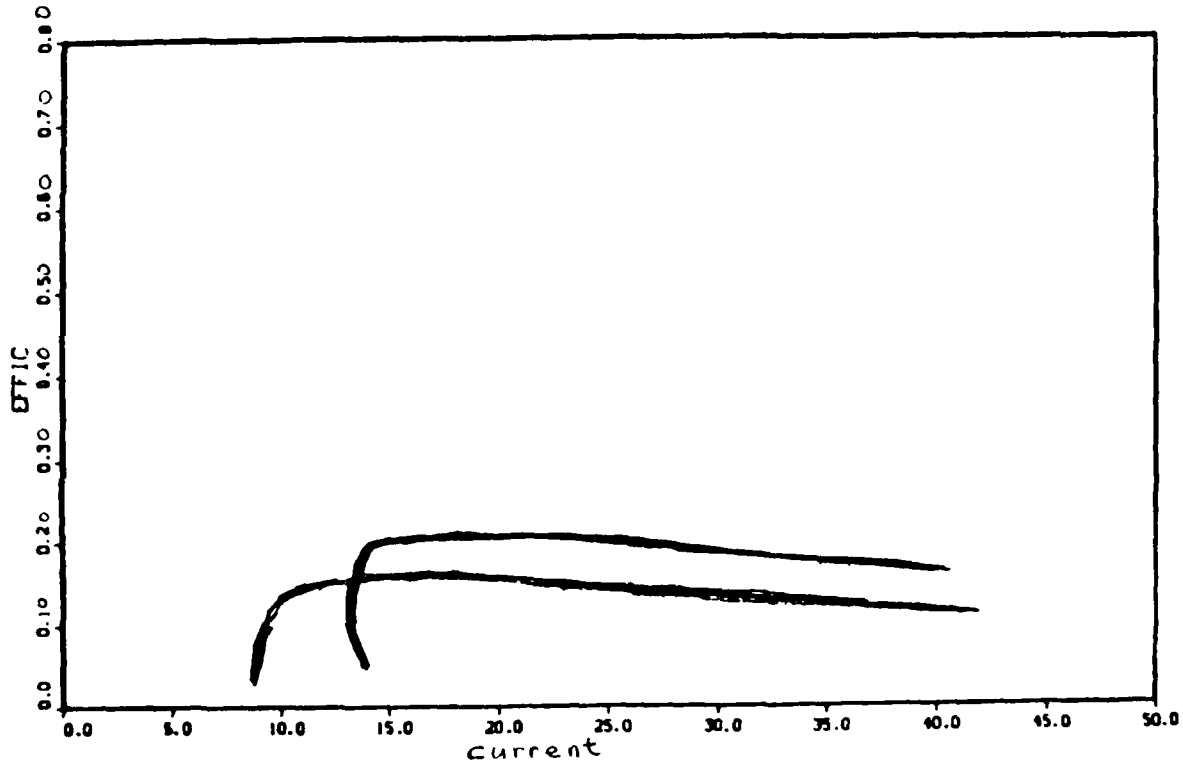

Figure 4 Efficiency versus current for Ω_c/ω_c=1.995, 2.010

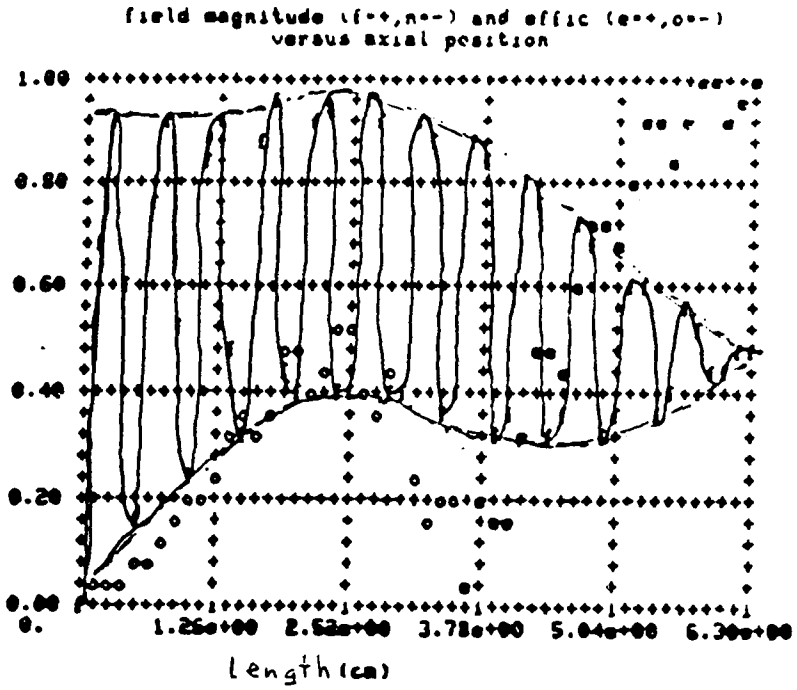

Figure 5a Field profile versus distance for backward wave interaction. Frequency = 42.84GHz. Efficiency = 4.45% Length = 6.3 cm. Beam current = 25 amps.

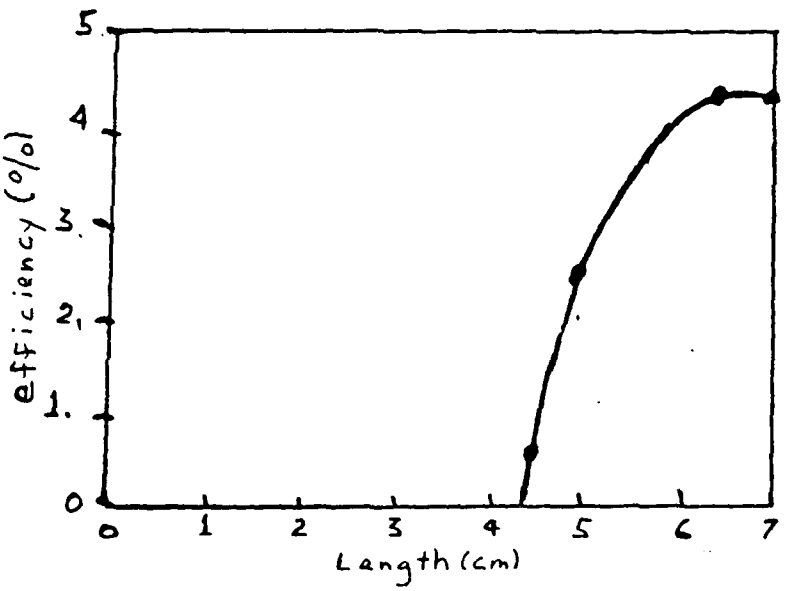

Figure 5b Efficiency versus interaction length for backward wave oscillation. Beam current = 25 amps.

APPENDIX 6

International Journal of Infrared and Millimeter Waves

HYBRID CYCLOTRON INSTABILITY IN A FREE ELECTRON LASER WITH AN AXIAL MAGNETIC FIELD

T. H. Kho and A. T. Lin

Physics Department
University of California
Los Angeles, California 90024

Received April 20, 1987

The axial guide magnetic field in a free electron laser (FEL) is found to give rise to a "hybrid" FEL- cyclotron instability. This instability occurs at a modified second harmonic FEL frequency where the axial ponderomotive force is resonant with a natural frequency of electron beam axial motion in the combined wiggler and guide magnetic field High efficiency, in excess of 30 percent, and strong growth rate are observed.

I. Introduction

In many free electron laser experiments, an axial magnetic field is added to guide the electron beam into the interaction region.[1] This axial field represents a new degree of freedom of the system. Previous investigations on the impact of the axial field on wave-particle interactions have concentrated on the instability at the free electron laser resonance, and to a lesser extent, that at the cyclotron maser resonance.[2,3,4]

In this paper, we present results from computer simulations of a "hybrid" FEL-cyclotron instability that is found to occur at a modified second harmonic FEL resonance. A $1\text{-}^{2}/_{2}$ dimensional, relativistic, electromagnetic particle code[5] is used to simulate the interaction of a tenuous electron beam with the radiation field in a static magnetic field of the form,

0195-9271/87/0700-0753$05.00/0

$$\vec{B} = B_c\hat{z} + B_w(\hat{x}Cosk_wz + \hat{y}Sink_wz) \quad (1)$$

where B_c and B_w are the guide and wiggler field strengths, respectively, and $\lambda_w=2\pi/k_w$ is the wiggler period. This wiggler field is an approximation of the field near the axis of the bifilar helix configuration used in experiments,[1] and is accurate for $k_wr<<1$, where r is the radius of beam excursion about the axis. The equilibrium steady state orbits for this magnetic field configuration is given by,[6]

$$\vec{p} = p_0\hat{z} + p_w(\hat{x}Cosk_wz + \hat{y}Sink_wz) \quad (2)$$

where

$$p_w=\Omega_w p_0/(\Omega_c-k_wv_0), \quad \Omega_w=eB_w/\gamma_0 m_e c, \quad \Omega_c=eB_c/\gamma_0 m_e c,$$

and γ_0 is the initial Lorentz factor of the beam. The usual FEL resonance arises from the transverse oscillation which induces radiation at the Doppler shifted wiggler frequency $\omega=(k+k_w)v_0$. To understand the hybrid instability, we note that for small perturbations about the steady state in the combined wiggler and axial field, the electron orbit is stable (in the absence of an electromagnetic field), but now contains additional modes of oscillation, approximately given by,

$$p_x = p_wCosk_wz + p_\perp Cos(\Omega_ct+\phi) - qCos(2k_wz - \Omega_ct + \phi)$$

$$p_y = p_wSink_wz + p_\perp Sin(\Omega_ct+\phi) - qSin(2k_wz - \Omega_ct + \phi) \quad (3)$$

$$p_z = p_0 - \beta_w p_\perp Cos(k_wz - \Omega_ct + \phi)$$

$$\beta_w = p_w/p_0 \qquad q = \frac{1}{2}\beta_w^2 p_\perp$$

where $p_\perp$ and ϕ are constants of motion and $p_\perp<<p_w$ has been assumed. There is now a Larmour component to the electron motion and the axial velocity is no longer constant, but oscillates at the cyclotron and wiggler beat frequency.

The third term in eq.(3) for the transverse velocity arises from the coupling of the axial oscillation with $\vec{B}_w$, and gives a modified second harmonic FEL resonance, $\omega = (k+2k_w)v_0 - \Omega_c$. Electromagnetic waves with frequencies in the neighbourhood of this resonance are found to be unstable. This instability arises for the following reason. An EM wave with frequency, $\omega=(k+2k_w)v_0 - \Omega_c$, will produce an axial ponderomotive force $[-\frac{e}{c}\vec{v}_\perp \times \vec{B}_{EM}]$, which is resonant with the natural frequency of beam axial oscillation.

$\Delta_a = |k_w v_0 - \Omega_c|$, (eq.3). For small but finite Δ_a, this resonant ponderomotive force can greatly amplify the axial oscillation in the electron motion, which, through its cross product with $\hat{B}_w$, drives a transverse current that reinforces the radiation at $\omega=(k+2k_w)v_0-\Omega_c$. This resonant amplification of electron axial oscillation has been observed in our simulations.

II. Simulation Results

In order to make the effect of this instability more transparent, simulations are performed keeping only one k-mode of the radiation field at a time. This is equivalent to simulating an amplifier system. A high efficiency regime appears to exist for EM waves that are simultaneously resonant with both longitudinal and transverse second harmonic electron oscillations. This occurs when $(2k_w v_0 - \Omega_0) = (\Omega_0 - k_w v_0)$ or $\Omega_0/k_w v_0 = 1.5$. Results for this case are shown below for the following parameters:

$\gamma_0 = 3.0$ $\quad \Omega_w/k_w v_0 = 0.12$ $\quad \Omega_c/k_w v_0 = 1.44$
$v_0/c = 0.91$ $\quad v_w/c = 0.25$

Figure 1 shows the dispersion diagram for EM waves propagating along the axial magnetic field in a plasma with drift velocity v_0. Note that the right polarized slow cyclotron wave is resonant with the $\omega=(k+2k_w)v_0-\Omega_c$ line at $k=6$ and with the FEL mode $\omega=(k+k_w)v_0$ near $k=10$ $(k=k/k_w)$. Not shown is the $\omega=(k-k_w)v_0+\Omega_c$ line which is parallel to, and just slightly below $\omega=(k+2k_w)v_0-\Omega_c$; it intersects the cyclotron wave at $k=5$. The right polarized fast EM wave is nearly coincident with the Doppler-shifted cyclotron resonance, $\omega=kv_0+\Omega_c$, for all values of k shown.

Exponential growth in the EM wave occurs for the whole range of k in figure 1. Maximum growth rate occurs at $k=6$, $w=5.82$ where the cyclotron wave and $\omega=(k+2k_w)v_0-\Omega_c$ intersect (fig.1), with a value of $0.076\omega_p$ $(w=\omega/\omega_p$, $\omega_p^2=4\pi ne^2/m_e)$, while maximum efficiency occurs at $k=5$. Figure 1b shows the evolution of the radiation field at $k=5$ and $k=10$. Figure 2a shows the power spectrum at saturation for $k=5$, 8, and 10. The power spectrum for $k=5$ shows the excitation of the right polarized cyclotron wave by the hybrid FEL- cyclotron resonance. For $k=8$, two instabilities are present. The lower frequency peak in the power spectrum corresponds to the right polarized slow cyclotron

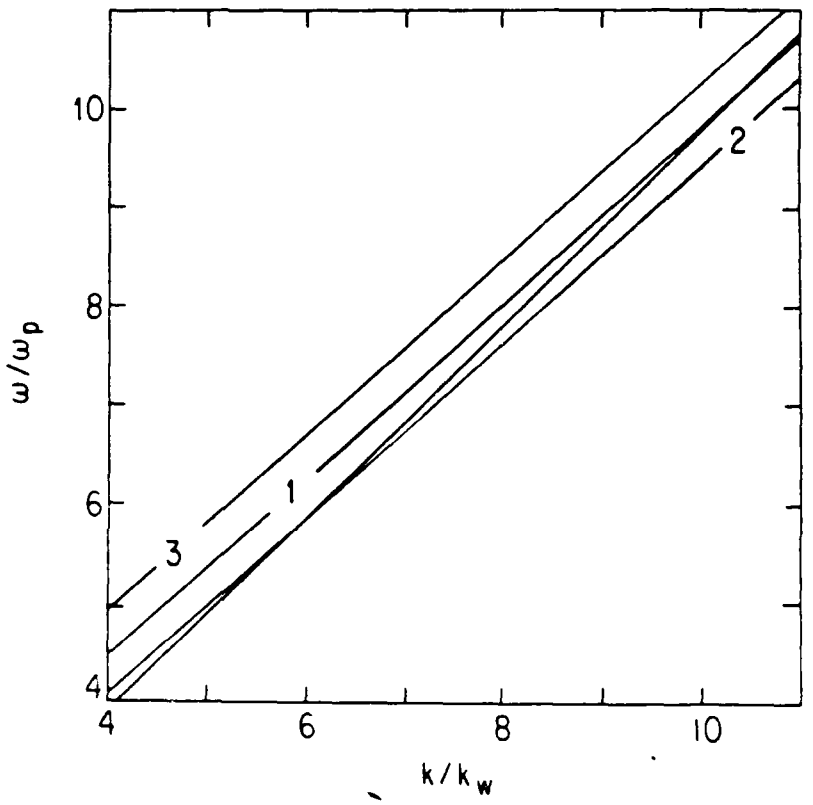

Figure 1. Dispersion diagram for Ω_0=1.28, γ_0=3.0 and β_0=0.91. Lines shown: $\omega=(k+k_w)v_0$ (1); $\omega=(k+2k_w)v_0-\Omega_0$ (2); right polarized fast EM (3), and slow cyclotron EM (unlabelled) waves.

wave excited by the hybrid resonance. The higher frequency peak is the FEL mode $\omega=(k+k_w)v_0$. For k=10, only one mode is evident. This is at the FEL resonance, and the growth rate, at $0.037\omega_p$, is about half that of the hybrid instability (fig. 2b). Conspicuously absent from these simulations is any sign of an instability at the Doppler-shifted cyclotron resonance, $\omega=kv_0+\Omega_c$, even though the right polarized fast EM wave frequency is very close to this resonance for the values of k here.

In an FEL instability, the electron beam is bunched

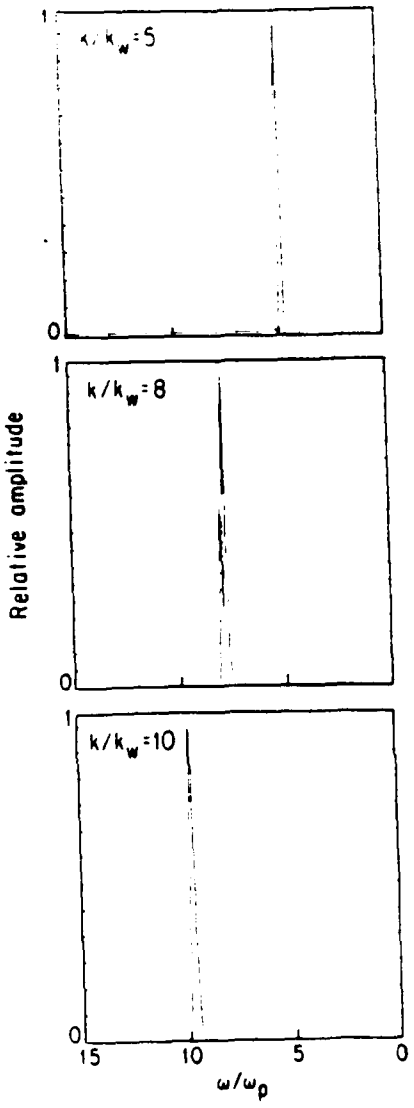

Figure 2a. Power spectrum at k=5, 8 and 10, at saturation.

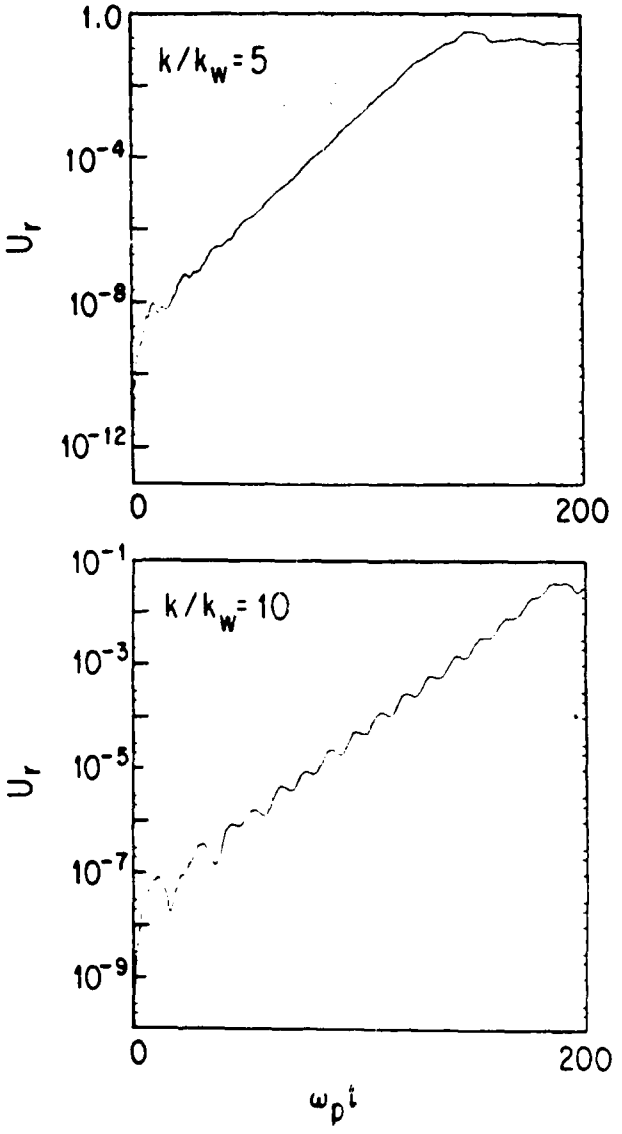

Figure 2b. Time evolution of radiation field at $k=5$ and $k=10$. $U_r = E_k^2(t)/[4\pi n m_e c^2(\gamma_o-1)]$ is the ratio of radiation to beam kinetic energy densities.

axially by the ponderomotive force at a periodicity of $k+k_w$ (and its harmonics). This occurs here, but in addition, a well defined change in the pitch of the electron beam is observed in the evolution of the second harmonic instability at $k=5$ (and also at $k=6$). Figure 3 displays the azimuthal location of electrons about the axis, parameterized by $\theta_i=\tan^{-1}(p_{yi}/p_{zi})$, over one wiggler period, at the initial time (a), at $\omega_p t=140$ (just before saturation) for $k=5$ (b), and at $\omega_p t=250$ for $k=10$ (c). The electron beam, which initially is a helix with the same pitch as the magnetic wiggler, evolves, in the case of $k=5$, into a helix with a pitch of $k+2k_w$. This new pitch results from the strong transverse Lorentz force on the beam, provided by $\vec{B}_w$ and the large axial oscillation in velocity driven by the resonant ponderomotive force. At $k=10$, away from the hybrid FEL-cyclotron resonance, the electron beam preserves its initial helicity throughout the unstable wave growth. Electron bunching at $k+k_w$ can be seen for both $k=5$ and $k=10$.

Maximum efficiency is obtained at $k=5$, where 35 percent of beam kinetic energy is converted into radiation energy. This efficiency is high, although it is only about half of what might have been expected from the reduction in beam axial velocity at saturation, $v_s/v_0\approx 0.88$ ($v_s=v_z(\omega_p t=150)$). If all the loss in axial kinetic energy goes into radiation, the efficiency can be estimated from $\eta=(\gamma_0-\gamma_s)/(\gamma_0-1)\approx 0.7$ $(\gamma_s-1/\sqrt{(1-\beta_s^2)}$, $\beta_s=v_s/c)$. The reason for this discrepancy is that a large fraction of the axial kinetic energy has been converted into azimuthal energy. The mean transverse velocity has increased by about a factor of two at saturation over its initial value.

As noted above, at $k=5$, the cyclotron wave is resonant with the axial oscillation of the beam (eq. 3). This appears to be relevant to the achivement of high efficiency here. Figure 4 shows plots of kinetic energy $(\gamma-1)$ versus axial velocity of electrons at saturation, $\omega_p t=150$, and after saturation at $\omega_p t=270$, for $k=5$. The electrons are initially concentrated at the point $(\gamma-1)=2$ and $\beta_z=v_z/c=0.91$. The resonance line for $\omega=(k-k_w)v_z+\Omega/\gamma$ is shown in figure 4a, for $k=5$, $\omega=4.89$ (the observed radiation frequency), where $\Omega=eB_0/m_e c$. Electrons on this line have axial oscillations that are resonant with the EM wave. At saturation, the bulk of the electrons have been shifted down into the $(\gamma-1)$ vs. v_z phase space encompassing this line, suggesting some degree of autoresonance.[7] For the

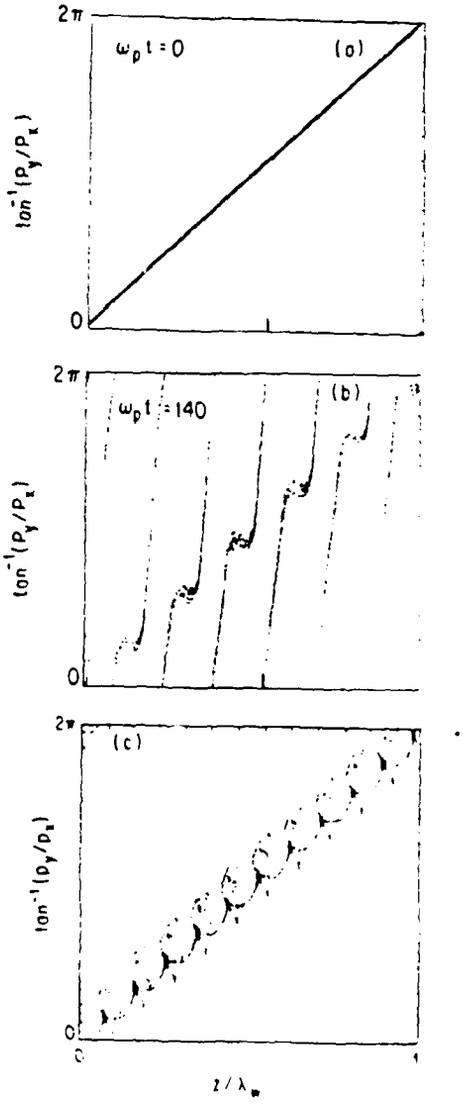

Figure 3. Change in pitch of electron beam at: (a) $\omega_p t=0$, (b) $k=5$, $\omega_p t=140$; (c) $k=10$, $\omega_p t=250$.

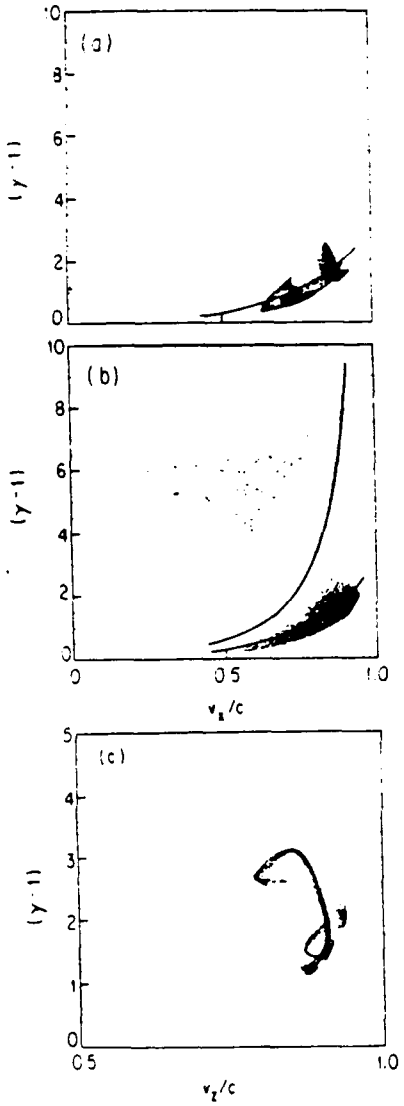

Figure 4.
Kinetic energy of electrons as a function of axial velocity: (a) k=5, $\omega_p t$=150, the continuous line is the $\omega=(k-k_w)v_o + \Omega/\gamma$ resonance line (k=5, w=4.89); (b) k=5, $\omega_p t$=270, the additional continuous line is the $\omega=kv_o+ \Omega/\gamma$ resonance line (k=5, w=4.89); (c) k=10, $\omega_p t$=250.

FEL resonance at k=10, the efficiency is only five percent and the (γ-1) vs. v_z plot (figure 4c) does not display the above feature.

After the hybrid instability saturated, some electrons continue to be accelerated by the EM wave to high energies (figure 4b). There are two distinguisible groups of electrons; one supporting the hybrid wave, the other being accelerated by it. The accelerated electrons appear to be confined to a fin shaped region in (γ-1) vs. v_z space, and bound at the upper v_z limit by the cyclotron autoresonance line, $\omega=kv_0+\Omega_0$, shown in figure 4b (phase velocity of EM wave at k=5 is ω/kc=0.998).

III. Conclusions

The introduction of an axial magnetic field into a helical wiggler field introduces the possibility of a natural low frequency mode of axial oscillation for the electron beam. When driven by a resonant ponderomotive force associated with an EM wave at the hybrid FEL-cyclotron resonance, $\omega=(k+2k_w)v_0-\Omega_c$, this axial oscillation can reach large amplitude so that when translated into transverse oscillation by $\vec{B}_w$, it serves to amplify the radiation. It is shown that some degree of autoresonance operate when the EM wave is also approximately resonant with the axial oscillation, enabling high efficiency, in this example, in excess of 30 percent, to be achieved. In a one-dimensional plasma, this (empirical) condition (Ω_c/k_wv_0~1.5) restricts the hybrid resonance to the slow cyclotron wave. However, this restriction is not necessary in a waveguide configuration, where, for sufficiently large Ω_c, the hybrid resonance can occur on a fast EM wave. The efficiency here compares very favourably with a cyclotron maser operated near autoresonance. For a Lorentz factor of γ_0=3, the expected efficiency of a cyclotron maser is about 20 percent, and for a relativistic gyrotron[8], is about 15 percent. However, to obtain optimum efficiency, the electron beam has to be injected with high uniformity in azimuthal velocity, which is technically difficult to achieve. Furthermore, the gain near autoresonance ($\omega/k_z c$) in a cyclotron maser is very small. In contrast, for the hybrid instability, no prior tailoring of beam transverse velocity is needed, and the gain is relatively high. These advantages makes the hybrid

instability a potentially attractive alternative to the cyclotron maser as a high efficiency microwave source.

Acknowledgements

This work was supported by ONR, AFOSR under contract No. F49620-85-K-0021, and NSF under contract No. ECS 86-03644.

References

(1). S.H. Gold, W.M. Black, H.P. Freund, V.L. Granatstein, R.H. Jackson, P.C. Efthimion, and A.K. Kinead, Phys. Fluids 26 2683 (1983).

(2). A.T. Lin, Chih Chien Lin, T. Taguchi, and W.W. Cheng, Phys. Fluids 26 3 (1983).

(3). Wayne A. McMullin and Ronald C. Davidson, Phys. Rev. A 25 3130 (1982).

(4). H.P. Freund, P. Sprangle, D. Dillenburg, E.H. da Jornada, B. Liberman, and R.S. Schneider, Phys. Rev. A 24 1965 (1981).

(5). A.T. Lin, J.M. Dawson, and H. Okuda, Phys. Fluids 17 1995 (1974).

(6). L. Friedland, Phys. Fluids 23 2376 (1980).

(7). A.T. Lin, Int. J. Electronics, 57 1097 (1984).

(8). A.W. Fliflet, NRL Memorandum Rep. No. 5598 (1985).